Miniaturised Wireless Power Transfer Systems for Neurostimulation: A Review

Gian Luca Barbruni [ID], Paolo Motto Ros [ID], *Member, IEEE*, Danilo Demarchi [ID], *Senior Member, IEEE*,
Sandro Carrara [ID], *Fellow, IEEE*, and Diego Ghezzi [ID], *Member, IEEE*

Abstract—In neurostimulation, wireless power transfer is an efficient technology to overcome several limitations affecting medical devices currently used in clinical practice. Several methods were developed over the years for wireless power transfer. In this review article, we report and discuss the three most relevant methodologies for extremely miniaturised implantable neurostimulators: ultrasound coupling, inductive coupling and capacitive coupling. For each powering method, the discussion starts describing the physical working principle. In particular, we focus on the challenges given by the miniaturisation of the implanted integrated circuits and the related ad-hoc solutions for wireless power transfer. Then, we present recent developments and progresses in wireless power transfer for biomedical applications. Last, we compare each technique based on key performance indicators to highlight the most relevant and innovative solutions suitable for neurostimulation, with the gaze turned towards miniaturisation.

Index Terms—Capacitive link, implantable medical device, inductive link, miniaturisation, neuroengineering, neurostimulation, ultrasound link, wireless power transfer.

I. INTRODUCTION

NEUROLOGICAL and mental disorders are medical conditions affecting a considerable portion of the society, whose impact can be alleviated by bioelectronics and neuroprosthetics medicine. Implantable neural prostheses, such as deep brain stimulators [1], cochlear implants [2], nerve stimulators [3], spinal cord stimulators [4], visual prostheses [5] and cortical stimulators [6] are example of clinically adopted neurotechnology to revert impaired or lost functions.

Gian Luca Barbruni is with the Medtronic Chair in Neuroengineering, École polytechnique fédérale de Lausanne, 1202 Geneve, Switzerland, with the Integrated Circuits Laboratory (ICLAB), École polytechnique fédérale de Lausanne, 2002 Neuchâtel, Switzerland, and also with the Department of Electronics and Telecommunications (DET), Politecnico di Torino, 10129 Turin, Italy (e-mail: gianluca.barbruni@epfl.ch).

Paolo Motto Ros and Danilo Demarchi are with the Department of Electronics and Telecommunications (DET), Politecnico di Torino, 10129 Turin, Italy (e-mail: paolo.mottoros@polito.it; danilo.demarchi@polito.it).

Sandro Carrara is with the Integrated Circuits Laboratory (ICLAB), École polytechnique fédérale de Lausanne, 2002 Neuchâtel, Switzerland (e-mail: sandro.carrara@epfl.ch).

Diego Ghezzi is with the Medtronic Chair in Neuroengineering, École polytechnique fédérale de Lausanne, 1202 Geneve, Switzerland (e-mail: diego.ghezzi@epfl.ch).

Clinically adopted implantable neural prostheses follow a very stereotyped design principle: a micro-electrode array (MEA) in contact with the tissue connects to an implantable electronic unit (IEU) via a cable. The IEU is a signal processing unit for neuronal recording or an implantable pulse generator (IPG) for neural stimulation or both. This design principle has its roots back to the first fully implantable battery-powered pacemaker [7]. Since then, several variations of this design principle were used in many successful applications, despite having several critical limitations. IEUs, cables and connectors are weak points of the system, often leading to failure. Besides, such an intricate design imposes several constraints on surgical procedures. Cables and connectors exert mechanical forces on the MEA and the tissue, therefore inducing long-term scarring. Cables are often transcranial or transcutaneous wires that might lead to post-surgical complications, such as infection. Power consumption, heat generation and high risk of failure in a wet environment due to leakage often limit IEUs. For instance, most of the clinically adopted implantable neurostimulators employ a wireless link for data and power transfer to the IPG, which is a bulky implantable medical device. Due to the size, IPGs cannot be located close to the target tissue. Instead, they are placed in a remote location and wires are used to connect them to MEAs for stimulation.

A technological challenge in neurostimulation is achieving a truly wireless stimulation with an array of freestanding smart electrodes, not relying on powered IPGs and wired connections. On the one hand, such smart electrodes should integrate all the required elements to receive power and operational commands. On the other hand, they should have a size compatible with the intended application (ideally smaller than 1 mm^3). The miniaturisation of the implantable device is crucial to achieve safe surgical implantation and long-term tolerability. For this reason, this review has the gaze turned toward the miniaturisation of the implant. Differently from other works [8], [9], [10] this review compares the advantages as well as the critical limitations of each powering method in designing a wireless link specifically for neurostimulation with extremely miniaturised implants.

II. WIRELESS POWER TRANSFER

Recently, there has been a growing interest in methods for wireless power transfer (WPT) in biomedical implants and neural prostheses.
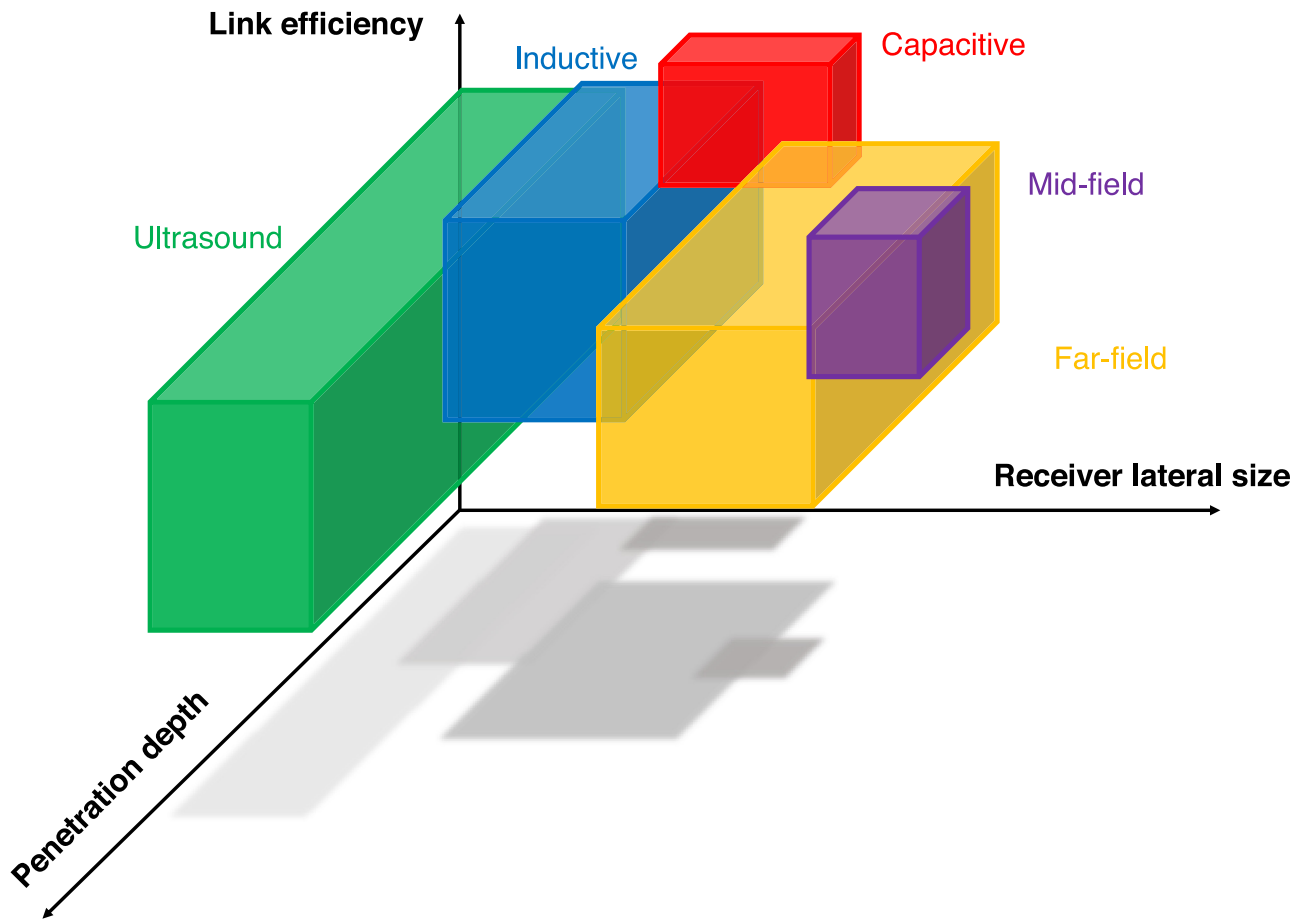
Fig. 1. Qualitative comparison of the methods for wireless power transfer. For each WPT method, the coloured box represents the area in which the trade-off between lateral size of the implant, penetration depth and link efficiency is optimised.

Fig. 1 qualitatively compares various WPT methods, as a function of three key performance indicators suitable for neurostimulation with miniaturised implants: the lateral size of the receiver, the penetration depth and the efficiency of the link. The latter is the ratio between the transmitted power and the power delivered to the load (PDL), excluding the efficiency of the drivers (Tx stage) and power manager (Rx stage). Five methodologies for WPT are compared: radio frequency (RF) radiation in the mid-field and far-field, inductive power transfer (IPT) and capacitive power transfer (CPT) in the near-field, and acoustic power transfer (APT). Each WPT method is illustrated only in the region of the graph in which the combination of the three key performance indicators is overall optimised to identify a trade-off suitable for neurostimulation with miniaturised implants. The analysis reveals that IPT, CPT and APT are the most suitable methods for neurostimulation with miniaturised implants.

Far-field and mid-field RF transmissions are appropriate for WPT to implants in the cm scale (or tens of mm), such as implantable pacemakers. The transmission is omnidirectional and, therefore, the signal loses its strength as it spreads further away from the source. As a consequence, the PDL decreases exponentially as the implant become smaller or deeper into the tissue. The goal is usually a trade-off between independence from direction and system efficiency. Fig. 1 highlights that WPT via far-field and mid-field has better performance when the distance between transmitter and receiver increases. As a rule of thumb, the performance is maximised when the size of the receiving antenna becomes comparable to the operating wavelength, which is to say that the operating frequency increases as the receiver size decreases. Therefore, when far-field or mid-field WPT is used for neurostimulation with miniaturised implants, a high-frequency signal is necessary and, as a consequence, the efficiency of the link will be strongly reduced due to high-frequency losses in the tissue. Most of the applications in the far-field aims at telemetry transmission at 2.45 GHz operating frequency, with a total size of some thousands of mm^3 [14], [15], [16]. Vorobyov and collaborators proposed a folded loop antenna for cochlear implants with a total implant volume larger than 3,000 mm^3 [17]. Manafi and Deng proposed a modified fractal antenna for passive deep brain stimulation reaching a volume of 640 mm^3 [18]. In the mid-field, Ma and Poon reported a RF powering technique to increase the gain of the transmitted power signal and to avoid spreading toward deep implanted stimulators in the tens of mm scale [19].

IPT, CPT and APT emerged as the most promising methods for WPT to miniaturised implantable neurostimulators. Fig. 2 highlights the working principles of the three selected WPT
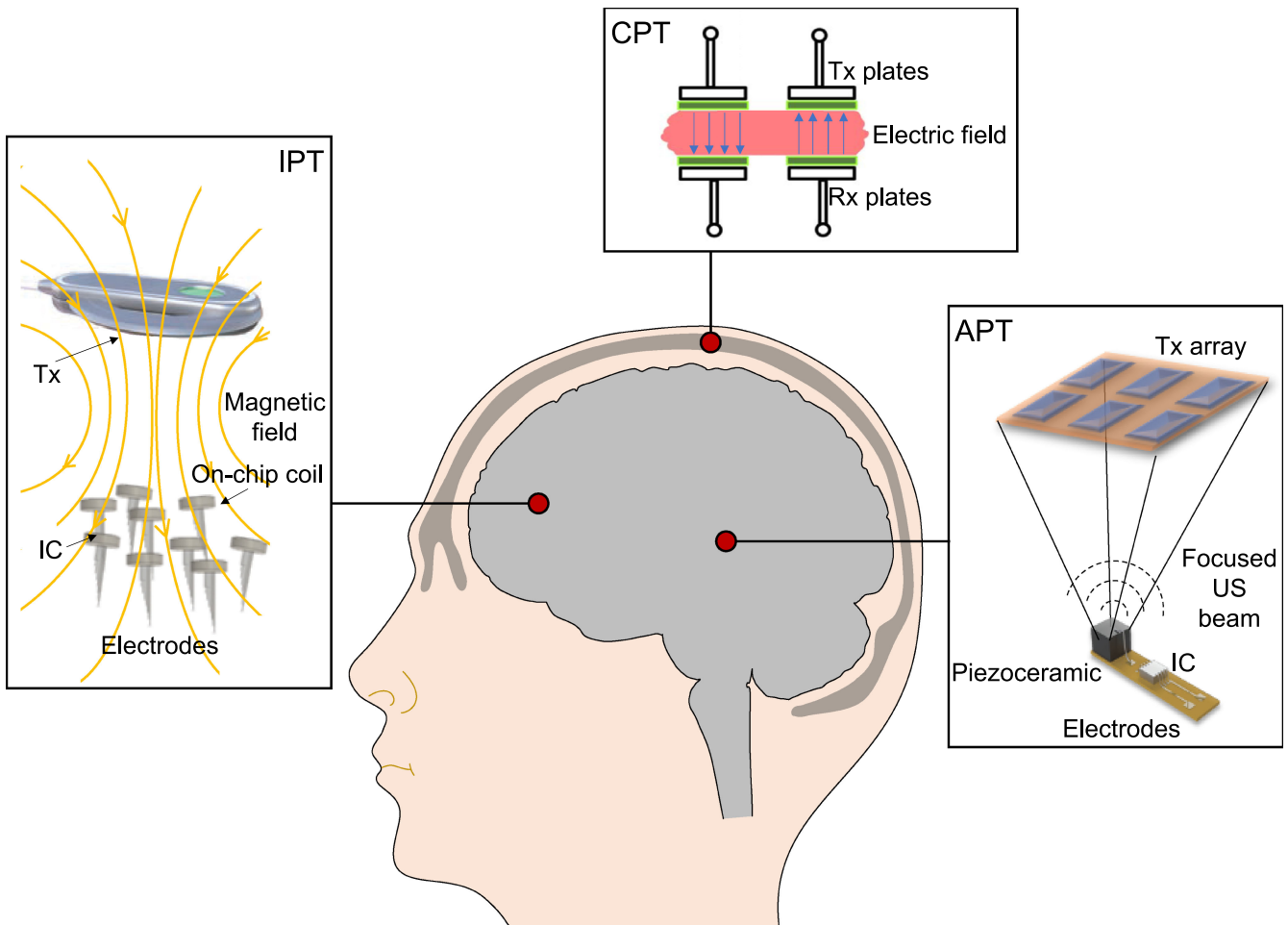
Fig. 2. Graphical representation of the three selected WPT methods and their general optimal working distance for neurostimulation with miniaturised implants. IPT requires at least one transmitting coil and one receiving coil, and works with magnetic coupling. Notably, one transmitting coil can address multiple receiving miniaturised implants. Scheme redrawn with permission from [11]; 2019 IEEE. The simplest CPT scheme has two couples of parallel plates (one for the transmitter and another for the receiver) separated by thin biological tissue, and works with electric field. Scheme redrawn with permission from [12]; 2011 IEEE. APT requires at least one piezoelectric transmitter or an array of transmitters generating a focused acoustic beam toward the piezoelectric receiver, inserted into the tissues. The piezoelectric receiver is an off-chip component that need to be bonded to the final Integrated Circuit (IC), leading to an overall increase of the implant volume. Scheme redrawn with permission from [13]; 2019 IEEE.

methods. APT has excellent performances for a single deep implant. Still, it usually requires off-chip components bonded together using a flexible printed circuit board (PCB), which increase the overall size of the implant. IPT is ideal for short-medium implantation depths, and it has the key advantage to allow powering multiple chips. CPT shows high performance for short-range implantation depths, but it has the key advantages of allowing integration in flexible substrates (similar to IPT) while avoiding the effect of electromagnetic interference (similar to APT). IPT has been largely investigated over the last decades; therefore, it is the most used WPT method by the scientific community. However, despite CPT and APT are relatively new techniques in the field, they already showed promising results toward wireless implantable devices in biomedical application and neural prostheses.

For each WPT method, we report the fundamental principles, and then we review the most innovative approaches showing potential towards neurostimulation with miniaturised implants.

In the concluding remarks, we compare the three methods highlighting their strengths and weaknesses.

III. INDUCTIVE POWER TRANSFER

IPT is a magnetic field powering method, using RF in the near-field region (operating frequencies from a few kHz to a few GHz). So far, IPT is the most commonly used WPT approach in implantable medical devices, since RF in the near-field is less attenuated by the human tissues.

A. Fundamental Principles

First, it is important to remark that the exposure to RF is tightly limited by standards. The maximum averaged Specific Adsorption Rate (SAR) for the human head is set by the Federal Communications Commission (FCC) to 1.6 W/Kg for 1 g of tissue mass measured during 6 minutes of exposure [20]. The
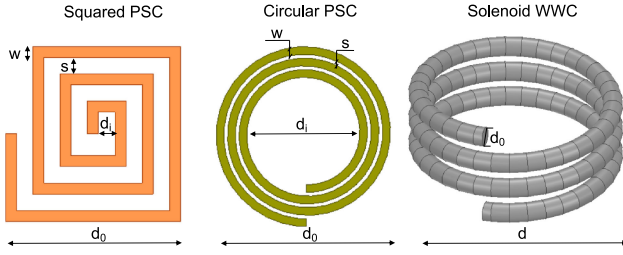
Fig. 3. Variants for the coil design: squared printed spiral coil (left), circular printed spiral coil (middle), and solenoid wire wound coil (right).
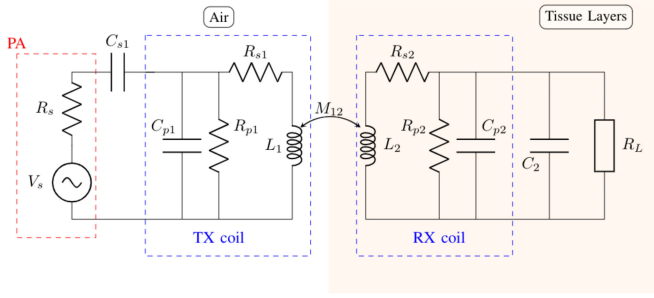

Fig. 4. General IPT link.

SAR is defined as in (1):

$$SAR = \frac{\sigma |E_{rms}|^2}{\rho} \tag{1}$$

where E_{rms} is the round value of the electric field; σ and ρ are respectively the tissue conductivity and density. Following the Maxwell's equation, it is possible to extract the electric field E from the magnetic field B as in (2):

$$\nabla \times E = -\frac{\partial B}{\partial t} \propto \omega_p I_1 \tag{2}$$

where ω_p is the operating frequency and I_1 is the flowing current. Therefore, several environments for the exposure's simulation assumed that the SAR is proportional to $(\omega_p I_1)^2$ [21]. Since the electric field is proportional to the current and the frequency, it is possible to increase the external current while keeping constant the SAR by proportionally decreasing the operating frequency of the link.

Another relevant parameter is the design of the coil, for which there are several possibilities, as sketched in Fig. 3. A first classification is between printed spiral coils (PSCs) [22] and wire wounded coils (WWCs) [23]. PSCs are characterised by high reliability and ease of manufacturing, in particular with micro- and nano-fabrication processes. However, the quality factor in PSCs is lower than in WWCs [24], [25]. The two geometries are also characterized by different key parameters. For a PSC, d_0 and d_i are respectively the outer and the inner diameters of the spiral, n is the number of turns while w and s are respectively the track width and spacing. Otherwise, for a solenoid WWC, d is the solenoid diameter, constant during the n number of turns, l is the conductor length, d_0 is the wire diameter and p is the winding pitch.

Fig. 4 shows an equivalent circuit for a general inductive coupling [26], in which all the losses terms for the coils are considered: L is the self-inductance value of the fabricated coil while R_S, R_P and C_P are respectively the series and parallel parasitic resistance and the parallel parasitic capacitance due to the coil geometry and some tissue parameters related to the surrounding environment (e.g. permittivity and conductivity). The other capacitors C_{s1} and C_2 are included as a matching element to achieve the same oscillation frequency of the two coils and maximise the power transfer efficiency (PTE). In the power amplifier stage of the primary coil, V_s is the voltage source generator followed by its intrinsic resistance R_s, while R_L is the load resistance in the secondary coil. M_{12} is the mutual coupling between the two coils. The subscripts 1 and 2 in Fig. 4 are respectively referred to the transmitter and the receiver coils. All these parameters depend on the physical fabrication of the coil (PSC or WWC), and for PSCs they also depend on the geometry (e.g. squared, circular or hexagonal). Schormans and collaborators [27] defined a table of expressions to extract the electrical parameters and to predict the electrical performances of the IPT link. In particular, for a squared PSC [28], the self-inductance L is defined as in (3):

$$L = \frac{1.27\mu n^2 d_{avg}}{2} \left[ln\left(\frac{2.07}{\varphi}\right) + 0.18\varphi + 0.13\varphi^2 \right] \tag{3}$$

where the permittivity is $\mu = \mu_r \mu_0$, the average diameter is $d_{avg} = (d_0 + d_i)/2$ and the fill factor is $\varphi = (d_0 - d_i)/(d_0 + d_i)$.

The other elements are the losses terms of the physical coil. The parallel parasitic resistance R_P in Fig. 4 is a material dependent parameter related to the dielectric loss δ_i, and it is significant at low frequencies and for materials with a small dielectric loss. The dielectric loss is generally defined starting from the loss tangent $tan(\delta_i)$ of each material i, which is related to its conductivity $\sigma_i = \varepsilon_0 \varepsilon_{r,i} \omega tan(\delta_i)$; where $\varepsilon_{r,i}$ is the relative dielectric constant of each dielectric layer i and ω is the frequency. R_P is not negligible for an external coil due to the low conductivity of air [26]. On the other hand, R_P could be negligible for implanted coils, due to the high dielectric loss in the tissue. For an external PSC coil, R_P as function of the frequency ω is approximated as in (4), where $K(k)$ is the complete elliptic integral of the first kind [29]:

$$\frac{1}{R_P(\omega)} = G_p(\omega) = \frac{\omega \varepsilon_0}{2}$$
$$\cdot \left[\varepsilon_{r1} \tan \delta_1 \frac{K(k_1')}{K(k_1)} \right.$$
$$+ (\varepsilon_{r2} \tan \delta_2 - \varepsilon_{r1} \tan \delta_1) \frac{K(k_2')}{K(k_2)}$$
$$+ \varepsilon_{r3} \tan \delta_3 \frac{K(k_3')}{K(k_3)}$$
$$+ (\varepsilon_{r4} \tan \delta_4 - \varepsilon_{r3} \tan \delta_3) \frac{K(k_4')}{K(k_4)}$$
$$\left. + (\varepsilon_{r5} \tan \delta_5 - \varepsilon_{r4} \tan \delta_4) \frac{K(k_5')}{K(k_5)} \right] \tag{4}$$

where, for the most general situation, the numeric subscripts (from 1 to 5) respectively correspond to tissue, top coating, air (for which $tan(\delta_3) = 0$), bottom coating and substrate [29].

The other lumped elements (series resistance R_S and parallel parasitic capacitance C_P) are always considered for both the transmitting and receiving coils.

R_S is geometry, material and frequency dependent, and it is the sum of two physical effects: the skin effect and the current crowding effect. The skin effect is the tendency of an alternating electric current to show the largest current density near the surface of the conductor, and to decrease its density deeper in the conductor. Therefore, the skin effect is stronger at higher frequencies. The current crowding effect is caused by eddy currents. When the magnetic field of an external turn penetrate another metal trace perpendicularly to its surface, eddy currents are generated within that trace in a direction orthogonal to the changes in the magnetic field according to Lenz's law [30]. The skin resistance for a PSC is defined as in (5):

$$R_{skin}(\omega) = R_{DC} \frac{t_0}{\delta \left(1 - e^{-\frac{t_0}{\delta}}\right)} \frac{1}{1 + \frac{t_0}{w}} \tag{5}$$

in which R_{DC} is the static resistance defined by (6) and δ is the skin depth defined by (7):

$$R_{DC} = \rho_c \frac{l_c}{w t_0} \tag{6}$$

$$\delta(\omega) = \sqrt{\frac{2\rho_c}{\omega\mu}} \tag{7}$$

in which t_0 is the thickness of the metal trace, ρ_c is the metal resistivity, μ is the metal permittivity and l_c is the length of the conductor according to (8) [31]:

$$l_c = 4nd_0 - 4nw - (2n+1)^2(s+w) \tag{8}$$

The Eddy resistance is defined by (9):

$$R_{eddy}(\omega) = \frac{1}{10} R_{DC} \left(\frac{\omega}{\omega_{crit}}\right)^2 \tag{9}$$

in which the frequency ω_{crit} at which the current crowding effect starts to become significant is defined by (10) taking in consideration the sheet resistance R_{sheet} [31]:

$$\omega_{crit} = \frac{3.1}{\mu_0} \frac{s+w}{w^2} R_{sheet} \tag{10}$$

Therefore, the series resistance can be defined by (11) as the sum of these two current effects:

$$R_S(\omega) = R_{skin}(\omega) + R_{eddy}(\omega)$$
$$= R_{DC} \left(\frac{t_0}{\delta \left(1 - e^{-\frac{t_0}{\delta}}\right)} \frac{1}{1 + \frac{t_0}{w}} + \frac{1}{10}\left(\frac{\omega}{\omega_{crit}}\right)^2\right) \tag{11}$$

C_P depends on the thicknesses of the different materials in contact with the coil [32]–[33], such as the metal trace itself, the substrate, the bottom coating, the encapsulation material (top coating) and the external environment (e.g. air, body tissue or body fluid). Even if an exhaustive definition of all the terms affecting the parasitic capacitance was proposed [26], a simplified

expression [24] defines the C_p as in (12):

$$C_p = (\alpha\varepsilon_{rc} + \beta\varepsilon_{rs})\varepsilon_0 \frac{t_0}{s} l_c \tag{12}$$

in which ε_{rc} and ε_{rs} are respectively the relative dielectric constants of the coating and the substrate layers [34], and (α, β) is experimentally assumed as (0.9, 0.1) in the case of air and a PCB substrate (FR4) [24].

In summary, the quality factor is calculated from the equivalent impedance of the lumped circuit by (13), and it represents an estimation of the coil capacity to generate high or low magnetic field, which is the ability to transfer more or less power.

$$Z(\omega) = \frac{R_S + j\omega L}{(R_S + j\omega L)(G_P + j\omega C) + 1} \tag{13}$$

Finally, from both the real and imaginary parts of the equivalent impedance Z of (13) it is possible to calculate the quality factor as $Q = \Im(Z)/\Re(Z)$. As we already mentioned, for implanted coils, the parallel parasitic resistance is negligible; thus the quality factor is simplified into (14):

$$Q(\omega) = \frac{\omega L - \omega C_p(R_S^2 + \omega_p^2 L^2)}{R_S} \tag{14}$$

The last term to be defined is the mutual inductance M_{12}, which is related to the coil geometry and distance. Several approaches were exploited over the last years to find the optimal expression for the mutual inductance. M_{12} can be calculated using complete elliptic integrals of first and second kind $K(k)$ and $E(k)$ [43]:

$$M_{12} = \theta \sum_{i=1}^{N_1} \sum_{j=1}^{N_2} M(x_i, y_j, d_{12}) \tag{15}$$

$$M(x, y, d_{12}) = \mu_0 \sqrt{xy} \left[\left(\frac{2}{\gamma} - \gamma\right) K(\gamma) - \frac{2}{\gamma} E(\gamma)\right] \tag{16}$$

$$\gamma = \sqrt{\frac{4xy}{(x+y)^2 + d_{12}^2}} \tag{17}$$

where x and y are the spatial coordinates and d_{12} is the distance between the coils. Another approach is to compute the value of the mutual inductance from the coil geometry and deriving the magnetic flux over a surface by superposing the effect of all the segments of the coil geometry, as in (18) [44]:

$$\mathbf{\Phi}_{ij} = \int_{S_j} \mathbf{B}_i \cdot d\mathbf{S}_j = \int_{S_j} B_{iz} \cdot d\mathbf{S}_j = \int_{S_j} B \cos\theta \cdot dS_j \tag{18}$$

However, the various methods are equivalent if the coupling distance between the two coils is sufficiently large (i.e. larger than 1 cm) [44].

Last, the PTE (η) and the PDL (P_L) could be defined by (19) and (20) [45]:

$$\eta(\omega) = \frac{k_{12}^2 Q_1 Q_{2L}}{1 + k_{12}^2 Q_1 Q_{2L}} \cdot \frac{Q_{2L}}{Q_L} \tag{19}$$

$$P_L(\omega) = \frac{V_s^2}{2R_1} \cdot \frac{k_{12}^2 Q_1 Q_{2L}}{(1 + k_{12}^2 Q_1 Q_{2L})^2} \cdot \frac{Q_{2L}}{Q_L} \tag{20}$$

TABLE I
INDUCTIVE POWER TRANSFER

Parameters	2015, [35]*	2016, [36]	2013, [37]*	2017, [38]	2019, [39]	2018, [40]	2018, [41]	2013, [42]
IPT Link	2-Coils	2-Coils	2-Coils	3-Coils	2-Coils	3-Coils	2-Coils	2-Coils
Rx size (mm^3)	1x1x1	1x1x1	1x1x1	1x1x1	0.3x0.3x0.004	0.5x0.5x0.0034	0.1x0.1xN/A	0.25x0.5x0.004
Rx material/Type	Cu/WWC	Cu/WWC	Cu/WWC	Cu/WWC	Al/On-chip	Cu/On-chip	Al/On-chip	Al/On-chip
Frequency	50 MHz	200 MHz	250 MHz	60 MHz	1.18 GHz	915 MHz	2 GHz	1.5 GHz
Distance (mm)	10	12	16	16	6.6	8	1.2	1
SAR (W/Kg)	1.6 (1g)	1.6 (1g)	1.6 (1g)	1.6 (1g)	0.15**	19.6 (10g)	N/A	N/A
Medium	Tissue	Tissue	Tissue	Air	Beef	Liquid phantom	Air	Air
PTE (%)	2.2	0.56	6.8	2.4	0.0019***	0.019-0.047	0.0016	0.021
PDL (μW)	2370	224	76.4	1300	55.5	95-235	100	10.5
Misalignment	No	No	No	Yes	No	Yes	No	No
R_{Load} (Ω)	N/A	5000	N/A	500	50	N/A	N/A	N/A

*Simulated; **@10 Hz pulsed input power; ***Rectifier included.

in which the coupling coefficient is derived by $k_{12} = M_{12}/\sqrt{L_1 L_2}$; Q_L is the load quality factor defined as $Q_L = R_L/(\omega L_2)$ and Q_{2L} is defined as $Q_{2L} = (Q_2 Q_L)/(Q_2 + Q_L)$.

Even if many optimization algorithms were proposed to maximize PTE and PDL [23], a good strategy is to design the link according to the application and, therefore, to its load resistance. The maximum PTE and PDL are achieved for a perfectly matched R_{Load}: this occurs for an R_{Load} usually smaller than 100 Ω. However, in biomedical implants with hundreds of μW of power consumption, R_{Load} is in the range of several hundreds of Ω [24]. Therefore, several L-match networks were proposed [23] to transform the R_{Load} imposed by the application, into a perfectly matched $R_{L,opt}$ defined by (21) [45]:

$$R_{L,opt}(\omega) = \omega_p L_2 Q_{L,opt} = \omega_p L_2 Q_2 \qquad (21)$$

If the imposed load is lower than $R_{L,opt}$, a series capacitor should be added into the secondary link. On the other hand, if R_{Load} is larger than $R_{L,opt}$, a series inductor is needed. However, the fabrication of a μm-sized inductor with high-quality factor is still a challenge.

B. IPT Links in Neural Applications

IPT is a useful method for WPT of a relatively large amount of power (i.e. a few hundreds of μW) to small mm-size receivers at a medium penetration depth (about 10–30 mm). In brain stimulation, the powering distance includes a relatively thick skull which has negligible attenuation of the RF wavelengths. Therefore, in the past years there was a strong research emphasis into the development of smaller implants powered via IPT and located into the neural tissue.

Table I reports the IPT links proposed in literature with a lateral size of the receiver smaller than 1 mm. The performances of the inductive link for small-size receivers strongly depends on

the operating frequency, which is typically in the 50–250 MHz range, for a millimeter size receiver. As the receiver become smaller, its self resonance frequency shifts toward the high frequency and the optimal operating frequency shifts accordingly in the same direction. Therefore, the link performance drastically decreases due to the high frequency losses of the human tissue.

Ibrahim and Kiani designed a 1 mm³ WWC receiver operating at 50 MHz (a relatively low frequency), to transmit 2.37 mW of power over a charging distance of 10 mm of human head tissues, under the SAR limit for RF exposure [35]. The simulations showed an overall efficiency of 2.2%, which is a promising result, even if the load resistance was not carefully taken into consideration. Only the optimal load condition was considered, which might not be the case for small-size and ultra low-power ICs. Similarly, Moradi and collaborators [37], simulated a 2-coils configuration for wireless transmission of 76.4 μW across a 12 mm of head tissues with the same wounded receiver size of 1 mm³ using a 250 MHz carrier frequency and reaching a 6.8% of PTE (always below the SAR limit). Again, the load resistance was not carefully taken into consideration.

The effect of the load resistance was considered by Ahn and Ghovanloo which designed and manufactured a 2-coils inductive link (similar structure of the previous ones [35], [37]) operating at 200 MHz, across a 12 mm of distance and transferring almost 224 μW with a total PTE of 0.56% [36]. Here a 5 kΩ loading resistance was proposed as equivalent impedance of a chip consuming almost 70 μW under a 0.6 V of voltage supply. The authors also proposed a design procedure to optimise the system by analysing both the total PTE and the SAR-constrained PDL. As a result, they introduced two new parameters to be optimised separately, when the size of the receiver coil is negligible compared to the transmitter coil, as for miniaturised implants. First, the authors defined the Power Reception Susceptibility (PRS) as the strength of the receiver to collect power under a certain
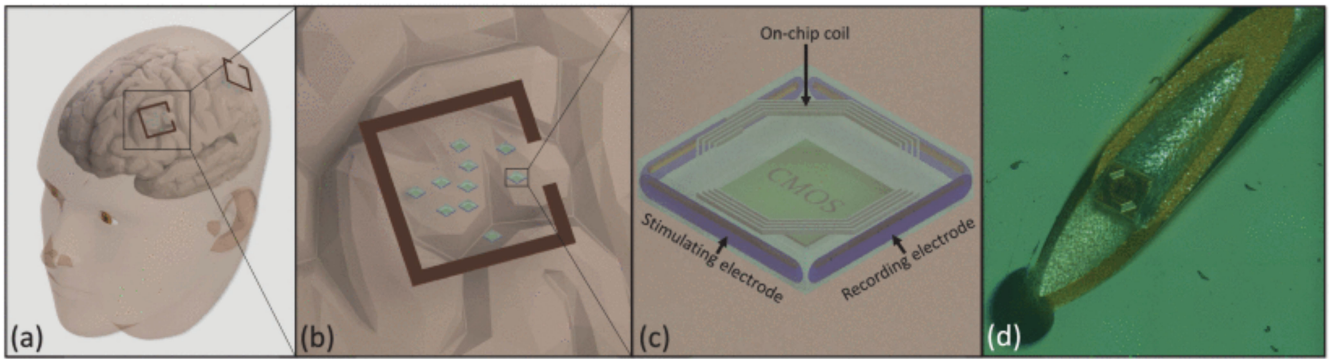
Fig. 5.   IPT in microbead injectable neural microstimulator. (a) 3D drawing of the scattered microbeads in the human cortex. (b) Close up view of the Tx coil. (c) The packaged microbeads with two electrodes for neurostimulation and two for recording. (d) Micrograph of the microbead, implantable with a 22G needle syringe. Reprinted with permission from [39]; 2019 IEEE.

magnetic field exposure. Second, they defined a new figure of merit (FoM) for the transmitter highlighting how strong it is coupled to the receiver, and minimising all the Tx-side losses. In particular, $Rx - PRS = Q_L\eta_{Rx}$ in which Q_L is the Rx loaded quality factor and η_{Rx} is the internal efficiency defined as $\eta_{Rx} = R_L/(R_L + R_S)$. Then, the Tx-FoM is defined as $Tx - FoM = Q_{TX}k^2$ in which Q_{TX} is the transmitter quality factor and k is the coils' coupling coefficient. Also, the design was optimised for the condition of a complete misalignment between the two coils, as previously suggested [46].

In these works, the receiver was always a solenoidal WWC, since it has the highest quality factor. However, further miniaturisation of implantable receivers would not be possible with this type of receiver [47]. Miniaturisation is hindered by the effect of the biological tissues, which have a high impact on the PTE and PDL [26] due to the attenuation effect and the higher parasitic capacitance values of the secondary side of the link. Sub-mm WWCs have some limitations. First, the low reproducibility due to manufacturing constraints; second, the post-processing required for the integration of the coil with the chip might reduce the device performance. On the other hand, on-chip coils have the advantages of allowing size reduction, higher reproducibility and reduction of the complexity by avoiding the bonding of the coil. The main drawback of on-chip coils is the lower quality factor if compared to the ones off-chip, due to the low thickness of the metal trace and the losses introduced by the silicon substrate. On-chip coils are typically manufactured on the ultra-thick top metal layer of the CMOS technology, and therefore they are usually designed with a PSC structure. Biederman and collaborators proposed a 2-coils link with a $250 \times 500 \ \mu m^2$ on-chip receiver coil integrated in a 65 nm CMOS processes to transmit almost $10.5 \ \mu W$ with a PTE of 0.021% across 1 mm of air at 1.5 GHz [42]. In a second study, the same technology was used to simulate a $100 \times 100 \ \mu m^2$ on-chip coil operating at 2 GHz for a powering distance of 1.2 mm [41]. Here, the authors provided an efficient equation-based optimisation procedure able to predict the efficiency of a 2-coils IPT system with an enormous advantage in terms of computational cost. Unfortunately, for this system the PTE was not provided. Recently, Khalifa and collaborators designed and manufactured

miniaturised and injectable neural stimulators [39], wirelessly supplied using on-chip inductors fabricated through 130-nm CMOS process. The receiver was a $300 \times 300 \ \mu m^2$ hexagonal-shape PSC operating at a maximum distance of 6.6 mm and reaching a PDL of almost $55.5 \ \mu W$ with a PTE of 0.0019% at 1.18 GHz (Fig. 5). The small PTE is justified since it also includes the effect of the rectifier, leading to an overall decrease of the system efficiency. Similarly, a $116 \ x \ 116 \mu m^2$ on-chip squared coil was manufactured using a 65-nm CMOS processes. The 2-coils architecture was able to transmit several tens of μW of power at high frequency (5.8 GHz), but at the optimised Tx-Rx distance of only 1 mm [48]. Unfortunately, the PTE was not specified by the authors. Nevertheless, they realised one of the smallest on-chip coil and tested the complete IC (batteryless, padless and crystalles) with a bi-directional communication to the external base station. Unfortunately, the penetration depth of these systems based on coils fabricated on-chip is still too short for neurostimulation applications.

All the described approaches were based on a 2-coils configuration. Therefore, the operating distance remained limited to a few millimeters while the operating frequency increased to the GHz range, where the tissue attenuation reduces the global performances of the link. The use of multiple coils to increase the overall efficiency of an inductive link was proposed already in 2005 by Atluri and Ghovanloo [49]. Besides increasing the PTE and the PDL, the other advantage of the 3-coils configuration is the reduced impact of misalignments and angular rotations [50], which is a critical point for 2-coils links (i.e. the PTE is almost zero when the two coils are rotated perpendicularly), and it is typically the case in neurostimulation with miniaturised implants. Ahn and Ghovanloo proposed an innovative configuration using a 3-coils structure to increase both the PTE and the PDL, and overcome the effect of the misalignment [38]. In this configuration, a WWC is used as a receiver, but two circular PSC are used as transmitter and resonator coils. A center frequency of 60 MHz was proposed to maximize both the PTE (2.4%) and the SAR-constrained PDL (1.3 mW) to power a load of 500 Ω over a powering distance of 16 mm (i.e. the typical averaged distance for an adult human head in the occipital area). Also, they demonstrated that a 3-coils system drastically reduces the SAR if
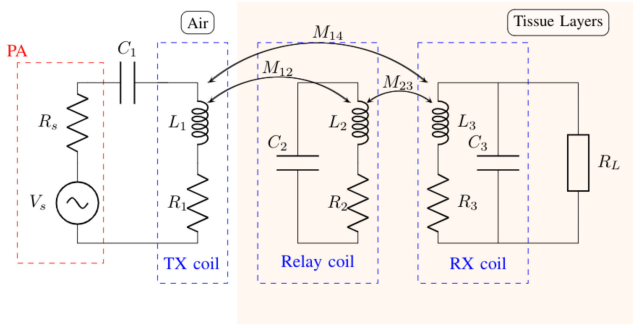
Fig. 6.   Three-coil design for an high efficient IPT link.

compared to a 2-coils system of an equivalent size. Recently, Jia and collaborators proposed a 3-coils IPT architecture to power a free-floating mm-sized device for both optical and electrical stimulation [51]. The maximum received power was 2.25 mW with a Tx-Rx distance of 5 mm, an operating frequency of 60 MHz and the WWC receiver used in [36]. The system on chip included the receiver coil, the IC realised with a $0.35\,\mu m$ processes, four off-chip capacitors, the electrodes and the micro-LEDs to provide the two types of stimulation. Therefore, the final implant volume increases to $2.5\ x\ 2.5\ x\ 1.5$ mm^3, due to the assembly process of all the off-chip elements.

Fig. 6 depicts a generic 3-coils configuration, in which, due to the insertion of the resonator coil (L_2) into the Tx-Rx trajectory, the PTE increases: $\eta_{3-coil} > \eta_{2-coil}$ [52]. By resonating at the same operating frequency of the link, the relay coil locally increases the magnetic field generated by L_1 thus increasing the coupling coefficient between the coils.

In particular, the efficiency of the 3-coils link could be expressed by (22):

$$\eta_{3-coil}(\omega) = \frac{k_{12}^2 Q_1 Q_2}{1 + k_{12}^2 Q_1 Q_2 + k_{23}^2 Q_2 Q_{3L}}$$

$$\cdot \frac{k_{23}^2 Q_2 Q_{3L}}{1 + k_{23}^2 Q_2 Q_{3L}} \cdot \frac{Q_{3L}}{Q_L} \qquad (22)$$

where, as for Q_{2L} of (19), Q_{3L} is defined as $Q_{3L} = (Q_3 Q_L)/(Q_3 + Q_L)$. Also, in a 2-coils configuration the coupling coefficient k_{12} is strongly reduced as the implant became smaller and the operating distance increases. Therefore, the PTE of the system is reduced since the coupling coefficient influences quadratically the PTE, as in (19). Moreover, it was demonstrated that k_{23} for a 3-coils configuration is 10 times larger than k_{13} [53], resulting into a higher PTE.

Recently, 3-coils architectures were largely investigated [54], [55] and exploited to power sub-mm devices at large distances [56] with an optimal operating frequency between 400 MHz − 2 GHz [57]. Lee, Laiwanna and collaborators proposed and realised a neural implants for neural recordings, called 'Neurograins', in which an ultra-thick copper coil is realized through TSMC foundry at 65 nm CMOS Low-Power process. The structure is a 3-coils configuration in which the receiver is a $500 \times 500\ \mu m^2$ PSC, $3.4\ \mu m$ thick, operating at 8 mm of Tx-Rx distance. The optimal operating frequency was 915 MHz of the

ISM (Industrial, Scientific and Medical) radio bands with a PDL of 235 μW and a PTE of 0.047% [40], [58]. The neurograin device ($650 \times 650 \times 250\ \mu m^3$) was recently validated with animal experiments for both neural recordings and stimulation [59]. Another solution was proposed by Ahmadi and collaborators using a two-tier configuration, with two arrays of inductive coils implanted above and below the skull and connected through cables [60]. The only remark to the ENGINI (Empowering Next Generation Implantable Neural Interfaces) system is the physical presence of a transcranial cable which might induce long-term side effects [11]. The same group proposes the use of EM-lens-enhanced inductive links for the resonator, using metamaterials to improve both the link efficiency and the covering distance of the link [61].

The limit for both the 2-coils and 3-coils system still remains the maximum input current (restricted by the FCC) that limits the maximum PDL. An interesting solution is the segmentation of the transmitting coil (and resonator coil for a 3-coils system), once its perimeter exceeds $\lambda_{medium}/10$ at the proper operating frequency [37], [38]. Another solution, proposed by Merli and collaborators [62], exploits flexible insulating layer for the implanted coils (e.g. polyamide) and an external insulating layer (e.g. silicon) directly in contact with the skin.

In conclusion, IPT was largely investigated and used in the field of biomedical implants, as well as in neural applications. The simplest 2-coils configuration was discovered to have critical limitation due to large Tx-Rx distance and small-size receivers. On the other hand, the 3-coils configuration with on-chip coils showed advantages for ultra-small size receivers and for large distances, which is typically the case in neurostimulation.

IV. CAPACITIVE POWER TRANSFER

Historically, CPT has attracted less attention than IPT for implantable medical devices and neurostimulation. However, after the first pioneering report [63], the use of CPT is now exponentially growing. CPT has several technical advantages compared to IPT. CPT is a low-cost technology, with high flexibility in manufacturing and reliable integration capacity in ICs. It is less affected by misalignments and angular rotations, and it shows negligible eddy current loss. Moreover, it shows almost the same performances in terms of link efficiency when implemented on flexible substrates [64]. Also, CPT is an interesting strategy to avoid the use of electromagnetic fields in case other sensitive devices are present. Last, capacitive coupling has the advantage of storing energy if a dielectric material is interposed between the capacitive plates.

A. General Principles

The capacitive coupling employs high-frequency electric fields for WPT. The coupling capacitance value depends on the area of the plates, the coupling distance and the dielectric material between the plates. The general electrical equivalent model for capacitive coupling is shown in Fig. 7, including two self-capacitance C_1 and C_2 and a generic equivalent mutual capacitance C_M represented by the two voltage-controlled current sources I_{M1} and I_{M2}.
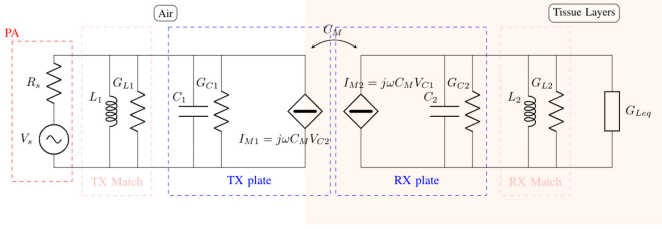
Fig. 7. Electrical equivalent model for a generic CPT link.

All the power losses components are expressed in term of their conductance compared to the resistance, in order to simplify the equations. Therefore, the physical losses of the capacitive plates are represented by G_{C1} and G_{C2} while L_1 and L_2 are the equivalent inductive resonance networks paired to their inductive power losses G_{L1} and G_{L2}. The equivalent inductive resonance networks are designed to perfectly resonate with the coupling capacitors. For the primary side, it is possible to compute the complex transmitted power S_{M1} according to (23):

$$S_{M1}(\omega) = V_{C1} \cdot (-I_{M1})^* = V_{C1} \cdot (-j\omega C_M V_{C2})^* \quad (23)$$

The mutual capacitance C_M is generally defined as the amount of charge stored in each plate per unit voltage difference between the two plates. The key parameters to be taken into account to design a capacitive link are the overlapping area of the two plates and their separation distance. From (23), it is possible to split the complex power S_{M1} into the active power P_{M1} and the reactive power Q_{M1} as:

$$\begin{cases} P_{M1}(\omega) = \omega C_M |V_{C1}| \, |V_{C2}| \sin\theta \\ Q_{M1}(\omega) = \omega C_M |V_{C1}| \, |V_{C2}| \cos\theta \end{cases} \quad (24)$$

in which the phase angle θ is a relevant parameter to minimise the conduction loss (having $Q_M \approx 0$). The optimal design of the matching network is an interesting strategy to adjust the phase angle (aiming at $\theta \to 90°$). Similar to IPT, the capacitive coupling coefficient k_c is obtained from (25):

$$k_c = \frac{C_M}{\sqrt{C_1 C_2}} \quad (25)$$

Overall, the CPT system efficiency could be expressed as follows:

$$\eta(\omega) = \frac{1}{\frac{\alpha + \frac{1}{\alpha} + 2}{k_c^2 Q_1 Q_2} + \frac{1}{\alpha} + 1} \quad (26)$$

in which α is the load ratio defined in (27), while Q_1 and Q_2 are the primary and secondary quality factors as expressed respectively in (28) and (29).

$$\alpha(\omega) = \frac{G_{Leq}}{G_2} \quad (27)$$

$$Q_1(\omega) = \frac{\omega C_1}{G_1} \quad (28)$$

$$Q_2(\omega) = \frac{\omega C_2}{G_2} \quad (29)$$

Moreover, as for IPT, the capacitive coupling may be categorized into resonant and non-resonant approaches. For high efficiency links the operating frequency needs to be increased because of the large forward impedance of the link due to the small tissue-based capacitance values [67]. Resonant CPT approaches are usually implemented to obtain efficient CPT at low frequencies.

B. CPT Links in Biomedical Applications

CPT is a relatively new emerging method for WPT in implantable medical devices. The first system for power and data transfer in implantable micro-systems was published in 2009 by Sodagar and collaborators [63]. The results of analytical calculations, simulations and experimental validations of the CPT link in air, revealed that the approach was expected to be more efficient compared to the other WPT methods, less susceptible toward RF interference and able to provide high-data-rate communication. Nevertheless, the main limitation was the relatively short-range distance (e.g. few millimeters) for both power and data communication.

After this first demonstration, other systems were proposed for WPT via CPT. Table II summarises and compares the smallest biomedical implants adopting WPT via CPT. The majority of these systems are sub-cutaneous implants with a chip lateral size larger than 5 mm and for a powering distance of less than 5 mm. Takhti and collaborators proposed the model of a capacitive link with a 5×5 mm^2 transmitter and receiver operating between 2 and 10 MHz for a maximum powering distance of a 3.5 mm with a thin layer of chicken breast interposed between the capacitive plates [65]. The system reached a total PTE of 48% at 10 MHz with a 100 kΩ load resistance. Hassan and collaborators proposed and simulated a multi-channel CPT system for data telemetry of implanted chips [12]. They observed a particular property of the capacitive link: the electric field distribution is dependent on the plates' geometry and their relative overlap. This result suggests that the lateral separation distance between the plates is an important parameter to be accounted for the optimisation of the PTE. Accordingly, they designed a 10×10 mm^2 transmitter and receiver plates, operating at 20 MHz to communicate with a sub-cutaneous implant with a 3.5-mm thick sheep skin between the primary and the secondary stages of the link.

Similar to IPT, the optimal operating frequency is a key parameter since the attenuation of the tissues increases at high frequencies. On the one hand, a relatively high frequency (190 MHz) is instead used in [67], with 5 mm of separation distance between the 40×40 mm^2 couple of transmitter plates and the 10×20 mm^2 receiving plate, reaching a maximum PTE of 66.4% and delivering 108.4 mW of power. On the other hand, it has been demonstrated that resonant CPT approaches enable efficient CPT at lower frequencies [70], [71]. In particular, an accurate circuit model for the coated capacitive elements around the tissue layer was recently validated [71]. Also, the authors highlighted the limitations in low-frequency CPT links proposing the further implementation of resonant capacitive links. Erfani and collaborators implemented a transcutaneous

TABLE II
CAPACITIVE POWER TRANSFER

Parameters	[65]	[12]	[66]	[67]	[68]	[69]
Year	2011	2015	2017	2017	2018	2019
Application	Sub-cutaneous	Sub-cutaneous	Sub-cutaneous	Sub-cutaneous	Sub-cutaneous	Deep-Brain
Tx size (mm^2)	5x5	10x10	20x20	40x40	20x20	15x15
Rx size (mm^2)	5x5	10x10	20x20	10x20	20x20	8x8
Powering Distance (mm)	3.5	3.5	5	5	3	15-30
Operating Frequency (MHz)	2-10	20	0.21	190	0.2-20	5-8
$R_{Load}(k\Omega)$	100	N/A	N/A	N/A	0.01-10	0.05
PTE (%)	48*	N/A	38.4	66.4	51.9	34.14
Max PDL (mW)	N/A	N/A	290	108.4	30.6**	N/A

*@ 10 MHz; **Lateral distance of plates L = 2 cm.

capacitive link based on a series of resonant converter using the two pairs of parallel plates as dielectric material replacing the standard tank capacitors of a standard IPT link. A 20×20 mm^2 transmitter and receiver were operating above resonance at 210 kHz to increase the PTE, reaching a total of 38.4% efficiency when delivering 105.5 mW of power under 11 V of direct current source from the external base station. Experimental validations showed a maximum of 290 mW delivered to the secondary side through a 5-mm thick beef slice [66]. One year later, the same group reported another capacitive link with the same size of the plates and a separation of 3 mm reaching a total of 51.9% efficiency and a maximum of 30.6 mW operating in a wide range of frequency, from 0.2 to 20 MHz and under a large load resistance range (0.01–10 kΩ) [68]. Also, the lateral separation L of the plates was evaluated, showing that both the PTE and the PDL can be maximised by increasing L. They demonstrated that by increasing the lateral separation from 2 cm to 70 cm the maximum PTE increases to 71.2% while the SAR-constrained PDL reaches 220.4 mW [68]. Moreover, they demonstrated a resonant tuned CPT link, made with flexible patches with an area of 20×20 mm^2 reaching almost 150 mW with an efficiency of 54% over 8 mm of chicken skin tissue [64]. The authors highlighted the importance of creating a system capable of providing the auto-resonant tuning of the frequency to maximize the efficiency of the system. Recently, they proposed an entire system for subcutaneous blood pressure monitoring [72]. The link has been realised by 20×20 mm^2 flexible copper plates, capable of reaching 65 mW of power with the adapted operating frequency of 2 MHz over 3 mm of tissue.

Narayanamoorthi proposed an innovative solution exploiting the CPT approach for a deep intracranial pressure sensor [69]. The author analysed a resonant capacitive-coupling WPT system with a multi-layer brain model and a $15 - 30$ mm penetration depth, obtaining a total PTE of 34.14%. They also analysed a new configuration with an intermediate plate showing an improved efficiency of 42.21%. The operating frequency was selected in the 5–8 MHz range and the amplitude phase-shift keying modulation technique was exploited for the up-link data communication. The receiver plates were 8×8 mm^2 in size while the transmitter plates were 15×15 mm^2 (Fig. 8). Another approach to increase the penetration depth of the CPT method is an architecture based on a four plate stacked-structure able to couple uniform current flow for deeply implanted medical devices [73]. Sedehi and collaborators proposed an implant with mm-sized parallel plates placed almost 15 mm inside into human thorax able to provide 10 mW of safety-constrained power under a load resistance of 30 Ω with an operating frequency of 6.7 MHz.

Even if CPT is an emerging WPT method, according to the current state-of-the-art, CPT is not yet mature enough for miniaturised implantable medical devices or neurostimulators. Recent developments in the field shows an outstanding performance for sub-cutaneous implants with a very high PTE, while the minimum size of the implant still remains limited by physical constrains. Since a couple of parallel plates is necessary on both sides of the link with a physical lateral separation (which is also demonstrated to be a key parameter to increase both the PTE and the PDL [12], [68]), the miniaturisation of the architecture to a sub-mm implant still remains an open challenge. Most of the systems involving CPT exploit the four-plate parallel structure [74], which is a main limitation for the system miniaturisation. Two recent studies [75], [76] proposed a single-wire configuration to eliminate the plate for the return path: a solution that might enable miniaturisation. However, a second couple of plates is usually needed for the closure of the electrical circuit. The absence of the plate for the return path is only an ideal situation, since the secondary stage will be coupled with the reference thanks to a return impedance Z_{ret} that is always present, and, moreover, it could be very high depending on the material through which the path will be electrically closed.
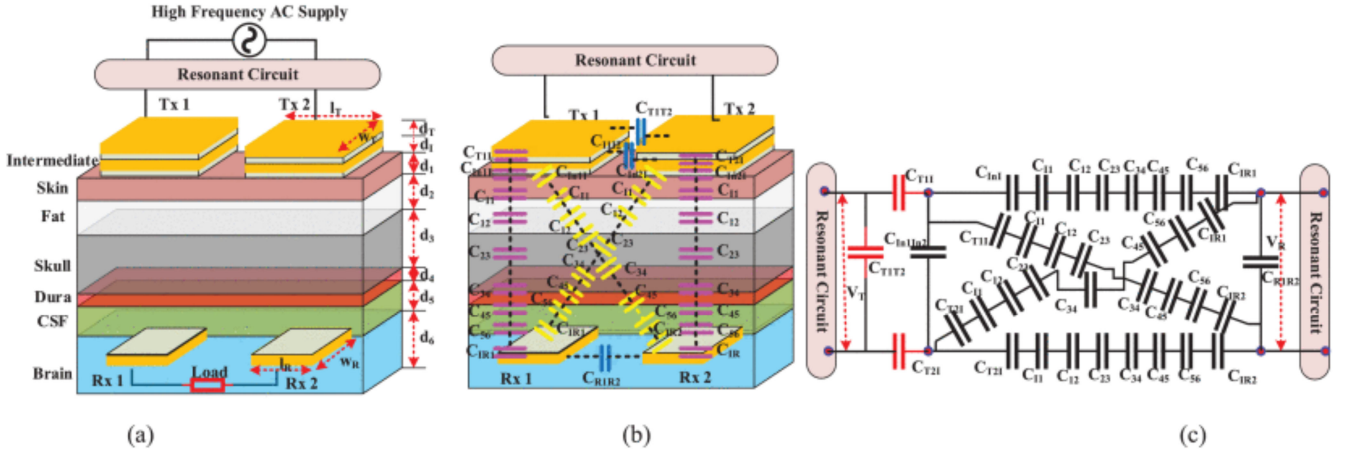
Fig. 8. CPT for intracranial pressure sensors. (a) RCCI (resonant capacitive-coupling with intermediate plate) structure. (b) Neural distribution of capacitance and (c) equivalent circuit model of capacitances between plates. Reprinted with permission from [69]; 2019 IEEE.
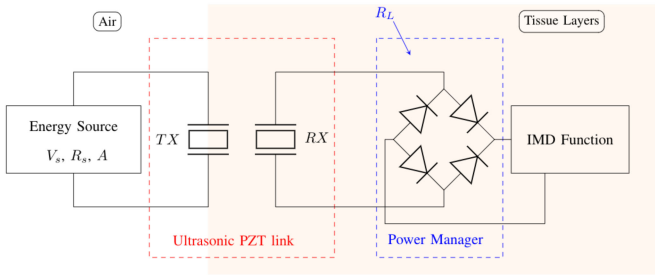

Fig. 9. Electrical equivalent model for a generic APT link.

V. ACOUSTIC POWER TRANSFER

APT is a popular method for WPT to implantable medical devices, mostly because acoustic waves (from hundreds of kHz to a few MHz) are less attenuated by the human tissues compared to RF, meaning that higher power can be transferred wirelessly to smaller receiver with a larger separation distance from the transmitter. Also, the maximum intensity allowed by the food and drug administration (FDA) is almost two order of magnitudes higher for APT than RF (respectively 720 mW/cm^2 and 10 mW/cm^2).

A. General Principles

Fig. 9 shows a generic ultrasonic wireless link. The external piezoelectric transducer is connected to an external energy source to generate the acoustic penetrating wave. On the other side of the link, the piezoelectric receiver converts mechanical vibrations into a voltage difference delivered to a load, which is expressed as the total load of the IC, including the rectifier and the regulator blocks of the power manager. In APT, there are three major losses terms. First, the tissue adsorption, derived from the Lambert-Beer law expressed by (30):

$$I_d = I_0 e^{-2\alpha d} \tag{30}$$

in which I_0 and I_d are the beam intensity before and after a thickness d of tissue and α is the adsorption coefficient, expressed in dB/(cm·MHz). Second, the mechanical to electrical power conversion efficiency (PCE) that is straightly dependent on the piezoelectric fabrication processes. In particular, piezoelectric micromachined ultrasonic transducers have better PCE compared to commercial off-the-shelf piezoelectric [77]. Third, the acoustic impedance mismatch is related to the direct contact of different materials, with different acoustic impedance values causing attenuation of the beam intensity due to reflections [78]. The impedance mismatch occurs at each interface (i.e skin-fat, fat-muscle, muscle-skull, skull-dura, dura-cerebrospinal fluid and cerebrospinal fluid-brain) but it is dominated by the reflection at the interfaces between the piezoelectric transducer and the skin, where $Z_{piezo} \approx 31\,MRayls$ and $Z_{skin} \approx 2\,MRayls$. Beam reflection is described by the reflection coefficient Γ, expressed in (31):

$$\Gamma = \left| \frac{Z_{tissue} - Z_{piezo}}{Z_{tissue} + Z_{piezo}} \right| \tag{31}$$

Solving (31) for the piezoelectric-skin interface, Γ is approximately equal to 0.9. Since the intensity of the transmitted beam is proportional to $(1 - \Gamma)^2$, this losses term become very important. In literature several techniques were proposed to overcome the acoustic impedance mismatch [78]. The simplest and widely used approach is called 'single layer technique', in which a single material is inserted between the piezoelectric and the tissue with a pre-defined thickness of $t_{match} = \lambda/4$. The material is appropriately chosen in order to respect (32):

$$Z_{match} = \sqrt{Z_{piezo} \cdot Z_{tissue}} \tag{32}$$

The main limitations of this technique are related to the limited number of biocompatible materials with a precise acoustic impedance (Z_{match}) and the need to account for the effect of the adhesive gel, that is always needed by the piezoelectric to adhered to the matching material. A possible solution for these limitations is the multi-layer approach. This technique, called 'multi-layer technique', is based on the multiplication of a chain

of transfer matrices. Each n material corresponds to a matching layer and it is represented by a 2×2 complex matrix T_n [79], as in (33) and (34):

$$T_n = \begin{bmatrix} \cos \theta_n & j Z_n \sin \theta_n \\ \frac{j}{Z_n} \sin \theta_n & \cos \theta_n \end{bmatrix} \quad (33)$$

Further:

$$\theta_n = 2\pi \frac{t_n}{\lambda_n} \quad (34)$$

in which t_n, λ_n and Z_n are the thickness (in m), the speed of sound (in m/s) and the acoustic impedance (in $MRayls$) of the n material respectively. If n materials are in contact between the transducer and the tissue, it is possible to define the product of the chain as the equivalent transfer matrix T_{eq}:

$$T_{eq} = T_1 T_2 T_3 T_4 = \begin{bmatrix} C_{11} & C_{12} \\ C_{21} & C_{22} \end{bmatrix} \quad (35)$$

Last, the equivalent acoustic impedance value is defined by (36):

$$Z_{eq} = \frac{C_{11} Z_{piezo} + C_{12}}{C_{21} Z_{piezo} + C_{22}} \quad (36)$$

The final matching is achieved when $Z_{eq} = Z_{tissue}$. Following these two strategies (single-layer and multi-layer), it is possible to increase the overall efficiency of the ultrasonic link without changing the design constraints, that are always fixed by the application. Another important aspect is the appropriate selection of the piezoelectric material, as the PCE is one of the losses term of the link. The direct and the inverse piezoelectric effects are governed by (37) and (38), as described in [80], [81]:

$$T = cS + hE \quad (37)$$

$$D = \varepsilon_r R + hS \quad (38)$$

in which, T is the stress, S the strain, E the electric field, D the electric displacement, c the elastic stiffness, h the piezoelectric coupling coefficient and ε_r the piezoelectric permittivity. Between all the material properties, in particular, for energy harvesting systems what is important is the electromechanical coupling factor, defined by (39):

$$k^2 = \frac{energy\ converted}{input\ energy} = \frac{\pi}{2} \frac{f_r}{f_a} \cot \left(\frac{\pi}{2} \frac{f_r}{f_a} \right) \quad (39)$$

in which, f_r and f_a are the series (or resonance) and parallel (or anti-resonance) frequencies. It was demonstrated that piezoelectric effects are different for different resonating modes [82]. The product between the resonant frequency and the thickness t of the piezoelectric defines a so called thickness mode frequency constant N_t (in Hz $\cdot$ m) as in (40):

$$N_t = f_r t \quad (40)$$

This parameter, usually specified by the manufacturer, is the starting point for designing an APT link, since it determines the resonance, as well as the anti-resonance, of the piezoelectric. Therefore, N_t is optimised according to the other application-constrained parameters (i.e. penetration depth, implant size and load) to select the most appropriate operating frequency [83].

One of the most important properties of the APT technique is the focusing of the acoustic beam generated by the Tx transducer. The focal zone is the point of transition between the near-field and the far-field regions [84], and it is mathematically expressed by the Rayleigh distance L as in (41):

$$L = \frac{D^2 - \lambda^2}{4\lambda} \approx \frac{D^2}{4\lambda} \quad (D \gg \lambda) \quad (41)$$

where, λ is the sound propagation wavelength in the medium and D is the diameter of the Tx piezoelectric transducer. To maximize the PTE, the Rx should be placed exactly at the focal point ($L = d_{Tx-Rx}$), that is also the zone in which the receiver is smaller.

In general, APT links are characterised following numerical approach (e.g. Huygens principle [85]) or through lumped element modelling, thanks to Krimholtz, Leedom and Matthae (KLM) [86] or Mason [87] equivalent circuit models. These models are valid for the majority of the APT characterisation while for a sub-mm design, a Finite Element Method (FEM) approach is preferred. As the aspect ratio (length/thickness) become higher, which is typically the case for ultra-small size piezoelectric receivers, the electrical equivalent models become less precise and therefore, more accurate FEM simulations should be used [88].

B. APT Links in Biomedical Applications

APT is a promising alternative to RF WPT because of safety considerations about electromagnetic interference. Moreover, as a rule of thumb, since the permitted input power level and the penetration depth are higher in APT compared to RF, more power can be transferred to a deeply implanted small receiver. Over the last 20 years, the use of piezoelectric transducer as electro-mechanical power converter in biomedical implants has followed an exponential trend. Table III summarised the state-of-the-art for piezoelectric transducers smaller than 5 mm^2.

In neurostimulation, the skull is the tissue with the highest adsorption loss, leading to strong attenuation of the acoustic beam. Compared to RF, for which the bone has practically a negligible influence, the strong ultrasound (US) attenuation of the bone results in low PTE. On the other hand, US carriers were demonstrated to pass the bone, making US technology suitable for neural recording and stimulation despite the low PTE. Also, a hybrid IPT-APT system was investigated to increase the overall WPT efficiency in miniaturised implants [94].

Denisov and collaborators reported an optimised disc-shaped piezoelectric receiver (diameter of 2 mm and thickness of 3 mm) operating at the optimal frequency of 1 MHz, for a powering distance of 10 cm and reaching a total efficiency of 0.02% [89]. They compared the acoustic link to an optimized inductive link with the same device size. The simulations showed that the PTE of the inductive link is three order of magnitude smaller for the same distance and similar operating frequency (13.56 MHz for IPT). The authors concluded that at small distances between transmitter and receiver (1 cm) IPT outperforms APT (for a receiver of 10 mm diameter). At larger distances (10 cm) the efficiency reduces significantly for both APT and IPT, but APT

TABLE III
ACOUSTIC POWER TRANSFER

Parameters	2017, [83]*	2010, [89]*	2015, [90]**	2015, [91]	2016, [92]**	2018, [93]**
Tx Diameter (mm)	10.8	20	12.7	20	6.35	20
Tx Thickness (mm)	1.05	3	N/A	1	2	N/A
Tx Backing	Air	Air	N/A	Air	N/A	Air
Tx Matching	Yes	Yes	Yes	Yes	Yes	Yes
Rx Diameter (mm)	1.2	2	1x1	1x5	0.127x0.127	0.6x0.6
Rx Thickness (mm)	0.25	3	1.4	1	0.127	0.6
Rx Backing	Silicon	Air	Air	Parylene-Coating	PCB	Air
Rx Matching	Yes	Yes	No	No	No	Yes
$R_{Load}(k\Omega)$	2.5	N/A	5-1000	5-100	10-100	0.4-10
Optimal Frequency (MHz)	1.8	1	1	2.3	5	1
Powering Distance (cm)	3	10	3	20	3	10
PTE (%)	2.11	0.02	N/A	0.4	0.002	0.23
PDL (μW)	N/A	N/A	360	2480	0.51	3000

*Simulation only; **Commercial Tx transducer.

has better performance than IPT. As the receiver gets smaller this efficiency gap increases and the distance after which APT outperforms IPT reduces (from 2.9 cm for a 10 mm receiver to 1.5 cm for a 5 mm receiver) [89]. These results indicate APT as the preferred choice for deep implants.

Song and collaborators reported an omnidirectional ultrasonic design for a deep implanted device (powering distance of 20 cm) using a 1×5 mm^2 receiver with 1 mm of thickness, working at the optimal frequency of 2.3 MHz and obtaining a maximum PTE of 0.4% while delivering a total of 2.48 mW of power under a load condition ranging from 5 to 100 kΩ [91].

Charthad and collaborators optimised a mm-size implant (thickness of 1.4 mm) operating at 1 MHz, reaching a total acoustic-to-electrical conversion efficiency higher than 50% and delivering a total of 360 μW at 0.72 mW/mm^2 (10% of the maximum FDA diagnostic limit) [90]. The system was tested for a load resistance ranging from 5 to 1000 kΩ and for a powering distance of 3 cm. In this work, it is suggested that it would be possible to deliver at least half the power to the receiver by reducing the size of the piezoelectric to 0.5 mm^3 while keeping the same input power intensity. Later, the same research group developed an end-to-end design for a sub-mm implantable receiver with a high efficiency single crystalline piezoelectric material that resonate in the range of 1–2 MHz [93]. They obtained a maximum efficiency of 1.93–0.23% for an implantation depth ranging from 6 to 10 cm and for a receiver width of 0.6 mm. Also, they proposed and simulated two different optimisation algorithms to maximize the PTE starting from the size-constraint due to the specific application. They measured the performance of different sub-mm cubic receivers
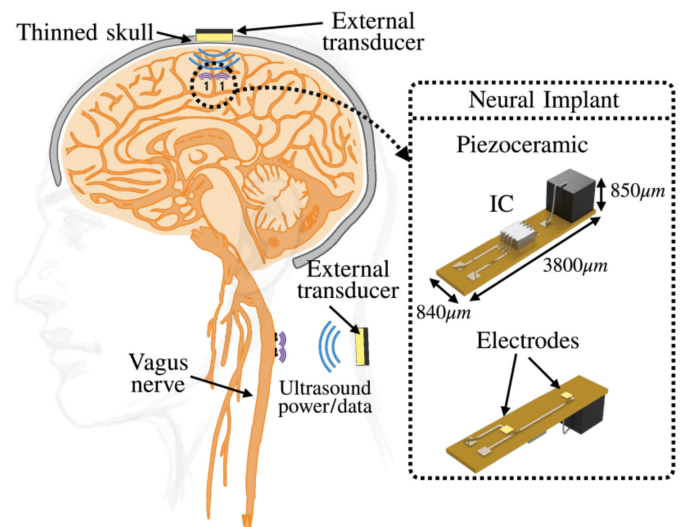

Fig. 10. APT in an untethered and free-floating implant for neural recording with a sub-mm^3 receiver. The neural implant is composed by single elements (piezoelectric receiver, sub-mm IC and recording electrodes) attached together via a flexible PCB to a final size of 2.71 mm^3. Reprinted with permission from [13]; 2019 IEEE.

with a lateral size ranging from 300 μm to 1 mm and adjusted the operating frequency to obtain a maximum of 0.048% for the smallest cube using a transmitter with a circular aperture of 2 cm and a prefixed load power of 3 mW. An alternative optimization procedure was proposed by Meng and Kiani, which proposed an high efficient US design for mm-sized implants [83]. The authors

also developed a disc-shaped piezoelectric receiver (1.2 mm in diameter and 0.25 mm in thickness) exploiting different matching strategies to reach a total efficiency of 2.11% for a powering distance of 3 cm, an optimal operating frequency of 1.8 MHz and an optimal load condition of 2.5 kΩ [83]. The authors concluded that the matching layer is a powerful method to increase the overall efficiency of the ultrasonic link.

Seo and collaborators developed the first unthetered free-floating sub-mm scale implantable device (called 'Neural Dust' [92]) to record electrophysiological activity, working both as power collector and up-link data communicator through backscattering. The system operates at 3 cm of depth and the measured efficiency for the smallest mote size (127 μm^3) was about 0.002% with a maximum of 0.51 μW when the input power density was kept to the maximum permitted by FDA (720 mW/cm^2). TheAPT system included a sub-mm custom-made Rx receiver operating with a commercial Tx transmitter. The experiments demonstrated that custom-made Rx receivers, with optimal focal point and input matching impedance, have an overall increase of both PTE and PDL of about two orders of magnitude. As the size of the receiver becomes smaller, the operating frequency must be increased since the resonating frequency of the piezoelectric transducer shifts to the highest frequencies as its thickness is reduced. The optimal operating frequency for that design was 5 MHz in a load condition ranging between 10 and 100 kΩ. The same working group developed a sub-mm free-floating implant for neural recordings using a cubic receiver with 750 μm of width [13] (Fig. 10), while recently they proposed a neural stimulator with acoustic powering and bi-directional data communication. The mm-sized neural stimulator, known as 'StimDust', incorporates a $750 \times 750 \times 750 \ \mu m^3$ lead zirconate titanate piezoceramic PZT transducer, chosen such as its series resonance was 1.85 MHz [95]. StimDust was implanted in the rat sciatic nerve to demonstrate its suitability as neurostimulation device. However, even if the piezoelectric is small, the final size of the StimDust device is 1.7 mm^3 since it includes the IC and the external energy-storage capacitor. The single elements are attached to a flexible PCB and encapsulated with parylene-C. The large size of the device precludes the use of StimDust in application requiring implants smaller than 1 mm^3. Also, the system is conceived to power a single element, hindering the possibility of having multiple stimulation sites.

A focused acoustic beam allows high penetration depth and deep placement of the receiver. On the other hand, when multiple ICs are required for multi-site stimulation, the physical separation between the implanted chips is a strong limitation. This problem could be addressed exploiting beam-forming systems [96], in which an array of Tx transducer is opportunely designed to interrogate several chips. Several ultrasonic beam-forming algorithms were proposed: from simple time delay and sum transmit beam-forming algorithms to more sophisticated ones suitable for high spatial resolution [97]. Since the Rayleigh distance strongly depends on both the Tx diameter and the sound propagation wavelength in the medium (41), another solution is increasing the Tx diameter and/or the operating frequency. In both cases, the focal point is pushed deeply inside in the tissue increasing the US near-field area available to power multiple

implants. Similarly, it is possible to move the implants toward the US far-field region (i.e. pushing the penetration depth even deeper than the Rayleigh distance) [83]. On the other hand, working away from the focal point limits both the Rx miniaturisation and the maximum PTE.

Another important issue of focused acoustic beams is the effect of angular rotation and misalignment on both the PTE and PCE [98]. Beam-forming systems were recently demonstrated to be an interesting and efficient strategy to minimise the negative effect of misalignment on the PTE [99]. Ibrahim and collaborators studied the spatial orientation effects on both inductive and ultrasonic link [100]. Their findings showed that when the implant size is smaller than 1.1 mm^2 ultrasonic systems are preferred [101] as well as when the penetration depth become larger than 10 mm [100] ultrasonic systems have better performances in terms of both PTE and PDL.

In summary, novel design strategies must be adopted to enable the miniaturisation of the transducers, including: i) increasing the optimal operating frequency [92], ii) exploiting acoustic repeaters using metamaterials (materials in which both effective density and bulk modulus are negative [102]) and iii) optimising beam-forming systems to interrogate a large number of chips at the same time.

VI. DISCUSSION

In this review paper, we highlighted three common methodologies exploited for wireless power transfer with a specific focus towards the miniaturisation of the implant for minimally invasive neurostimulation. In particular, we compared ultrasound, capacitve and inductive links by reviewing their operation principles and summarising relevant exploitation in biomedical implants.

Fig. 11 shows a side-by-side comparison among the IPT, CPT and APT systems presented in this review article (from Tables I, II and III) according to the three key performance indicators identified as relevant for neurostimulation with miniaturised devices: the lateral size of the receiver, the penetration depth and the efficiency of the link. Indicators were compared in pairs.

From the review results, it is possible to conclude that acoustic power transfer allows high penetration depth and high input power; therefore, it takes advantage of sub-mm^3 piezoelectric receivers to miniaturize the overall implant size. In particular, micromachined transducers emerged as the most efficient ultra-small-size receivers useful to the aim. Moreover, the large exposure limit allowed by the specific absorption rate allows for higher power on the transmitting stage, making acoustic power transfer suitable to target small and deep implants. This is a major advantage compared to inductive and capacitive methods, in which the maximum allowed exposure is a strong limiting factor, reducing the maximum power density on the transmitting stage and, therefore, the maximum power available to the implanted load. On the other hand, acoustic power transfer is constrained by issues related to fabrication, integration with μm-chips and high sensibility to misalignments and angular rotations. Also, acoustic transfer is not ideal when multiple
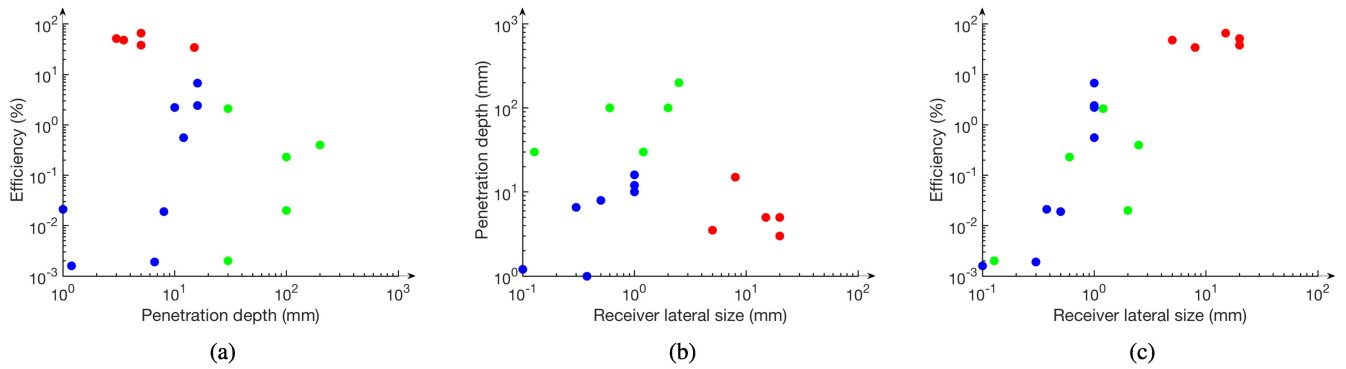
Fig. 11. State-of-art comparison among recent IPT (blue), CPT (red) and APT (green) miniaturised systems for WPT. To simplify the visual comparison, in each panel data have been plotted comparing two of the three parameters: efficiency vs. penetration depth (a), penetration depth vs. receiver lateral size (b) and efficiency vs. receiver lateral size (c). Data are from Tables I, II and III.

TABLE IV
COMPARISON OF METHODS FOR WIRELESS POWER TRANSFER

Feature	ULTRASOUND (APT)	CAPACITIVE (CPT)	INDUCTIVE (IPT)
Fabrication	Difficult (pMUTS)	Simple	Challenging (3-coils)
Costs	High	Low	Moderate
Integration on-chip	No	Simple	Simple (PSC)
Penetration depth	> 2 cm	< 1 cm	< 2 cm
Smaller Rx @ 2020	$0.75^3 \ mm^3$ [13]	$8x8 \ mm^2$ [69]	$0.09 \ mm^2$ [39]
PTE and PDL @ 2 cm	High	Low	Moderate
Effects on misalignment	High	Low	Moderate (3-coils)
SAR limit	High	Low	Low
Tissue attenuation	Low	High $\propto$ f	High $\propto$ f
Multiple IC problems	Focusing (Beamforming)	No	No
Electromagnetic interference	No	No	Yes

receivers are required since transmitting arrays of transducers and accurate beam-forming algorithms are needed.

On the other hand, capacitive power transfer is a low-cost technology, with an high flexibility in manufacturing and a reliable integration with ultra-small integrated circuits. Also, it is less affected by misalignments and angular rotations compared to acoustic methods. Capacitive systems have negligible eddy current loss and show interesting electromagnetic compatibility compared to inductive systems. It is also an interesting method for application with flexible substrates. A general disadvantage of the capacitive approach is the dependence of the efficiency of the link by the frequency. The frequency needs to be increased for efficient power transfer, but, in turn, higher frequencies increases losses and reduce penetration. On the other hand, recent results showed that resonant transfer approaches enable high efficiency at low frequencies too. Also, recent demonstrations of auto-resonant techniques further improved the functionality

of resonant capacitive links [103]. Yet, the miniaturisation of the coupling plates is still a challenge at the current state-of-the-art, which limits the minimum size of the receiver, as well as the maximum penetration depth.

As last, but not least, inductive link is the oldest and most used technique for wireless power transfer. Similar to capacitive, the efficiency of the link increases with the frequency; however, high frequency signals are more attenuated by the tissue. Therefore, innovative solutions were developed to improve the method compared to problems related to low efficiency and low power density to the load. For example, 3-coils structures were demonstrated to overcome the limits of 2-coils structures in terms of both efficiency and exposure-constrained density to load. The 3-coils architectures also make inductive systems less sensible to misalignments and angular rotations. Last, 3-coils systems further allow for the miniaturisation of the receiver. Although on-chip coils typically have the lowest quality-factor, they have

shown interesting advantages toward extreme miniaturisation: they allow direct fabrication of the receiving coil avoiding post-processing operations usually needed for the integration with μm-chips, and they present high manufacturing reproducibility.

All the presented methods have their unique advantages, since the most suitable method is always application-dependent. If the application requires a deep and small implant, for example in the case of deep brain stimulation or vagus nerve stimulation, power transfer by acoustic signals is the most suitable approach. On the other hand, if multiple receivers are required, for example for neurostimulation at multiple close sites (e.g. sensory restoration and spinal cord stimulation), capacitive and inductive links are the best choice. The power transfer by capacitive link usually presents high efficiency for large receivers at short distances (e.g. large subcutaneous implants) and it could be selected also to avoid electromagnetic interference. Otherwise, IPT links are preferred for intermediate depths, smaller implant and multiple implants, such as for high-resolution intra-cortical stimulation.

To conclude, Table IV provides general indications to select among acoustic, capacitive or inductive methods. Based on our analysis, each method presents advantages as well as limitations; therefore, it is not possible to uniquely select the most suitable wireless power transfer method for neurostimulation with minimally invasive miniaturised implants. In particular, the selection among the three methods strongly depends on the specific application-dependent parameters, such as the depth of the implanted receiver, the lateral size of the receiver, the number of independent implantable receivers and the total power required. Being so application-dependent, we have not extracted any single figure of merit to numerically compare in a clear, unique and visible way, the three methods.

VII. CONCLUSION

Different solutions proposed in literature for wireless power transfer were compared in this review article showing key performance indicators relevant for neurostimulation with minimally invasive miniaturised implants. At the very end, acoustic, capacitive and inductive links were identified as the most promising methods; however, the selection of a specific method strongly depends on the application. The latest developments and the recent innovative proposals in the field of wireless power transfer, especially for neurostimulation, are making the topic increasingly challenging and increasingly suitable toward miniaturised devices.

REFERENCES

[1] A. L. Benabid, S. Chabardes, J. Mitrofanis, and P. Pollak, "Deep brain stimulation of the subthalamic nucleus for the treatment of Parkinson's disease," *Lancet Neurol.*, vol. 8, no. 1, pp. 67–81, 2009.

[2] J. T. Rubinstein, "Paediatric Cochlear implantation: Prosthetic hearing and language development," *The Lancet*, vol. 360, no. 9331, pp. 483–485, 2002.

[3] S. Raspopovic *et al.*, "Restoring natural sensory feedback in real-time bidirectional hand prostheses," *Sci. Transl. Med.*, vol. 6, no. 222, 2014.

[4] F. B. Wagner *et al.*, "Targeted neurotechnology restores walking in humans with spinal cord injury," *Nature*, vol. 563, no. 7729, pp. 65–71, 2018.

[5] D. Ghezzi, "Retinal prostheses: Progress toward the next generation implants," *Front. Neurosci.*, vol. 9, p. 290, 2015.

[6] S. Niketeghad *et al.*, "Phosphene perceptions and safety of chronic visual cortex stimulation in a blind subject," *J. Neurosurgery*, pp. 1–8, 2019.

[7] O. Aquilina, "A brief history of cardiac pacing," *Images Paediatric Cardiol.*, vol. 8, no. 2, p. 17, 2006.

[8] R. Das, F. Moradi, and H. Heidari, "Biointegrated and wirelessly powered implantable brain devices: A review," *IEEE Trans. Biomed. Circuits Syst.*, vol. 14, no. 2, pp. 343–358, Apr. 2020.

[9] S. R. Khan, S. K. Pavuluri, G. Cummins, and M. P. Desmulliez, "Wireless power transfer techniques for implantable medical devices: A review," *Sensors*, vol. 20, no. 12, p. 3487, 2020.

[10] Y. Zhou, C. Liu, and Y. Huang, "Wireless power transfer for implanted medical application: A review," *Energies*, vol. 13, no. 11, p. 2837, 2020.

[11] N. Ahmadi *et al.*, "Towards a distributed, chronically-implantable neural interface," in *Proc. 9th Int. IEEE/EMBS Conf. Neural Eng.*, Mar. 2019, pp. 719–724.

[12] A. Hassan, C. Sawma, M. Hasanuzzaman, B. Gosselin, and M. Sawan, "Spatial carrier position modulation based multichannel capacitive link for bioelectronic implants," in *Proc. IEEE Biomed. Circuits Syst. Conf.*, Oct. 2015, pp. 1–4.

[13] M. M. Ghanbari *et al.*, "A Sub-mm 3 ultrasonic free-floating implant for multi-mote neural recording," *IEEE J. Solid-State Circuits.*, vol. 54, no. 11, pp. 3017–3030, Nov. 2019.

[14] H. Huang *et al.*, "RFID tag helix antenna sensors for wireless drug dosage monitoring," *IEEE J. Transl. Eng. Health Med.*, vol. 2, pp. 1–8, 2014.

[15] E. Y. Chow, Y. Ouyang, B. Beier, W. J. Chappell, and P. P. Irazoqui, "Evaluation of cardiovascular stents as antennas for implantable wireless applications," *IEEE Trans. Microw. Theory Techn.*, vol. 57, no. 10, pp. 2523–2532, Oct. 2009.

[16] F. Merli *et al.*, "Example of data telemetry for biomedical applications: An in vivo experiment," *IEEE Antennas Wireless Propag. Lett.*, vol. 11, pp. 1650–1654, 2012.

[17] A. Vorobyov, C. Hennemann, A. Vasylchenko, J.-D. Decotignie, and J. Baumgartner, "Folded loop antenna as a promising solution for a cochlear implant," in *Proc. IEEE 8th Eur. Conf. Antennas Propag.*, 2014, pp. 1735–1738.

[18] S. Manafi and H. Deng, "Design of a small modified minkowski fractal antenna for passive deep brain stimulation implants," *Int. J. Antennas Propag.*, vol. 2014, 2014.

[19] A. Ma and A. S. Poon, "Midfield wireless power transfer for bioelectronics," *IEEE Circuits Syst. Mag.*, vol. 15, no. 2, pp. 54–60, 2015.

[20] 2. IEEE Standards Coordinating Committee, "IEEE standard for safety levels with respect to human exposure to radio frequency electromagnetic fields, 3 kHz to 300 GHz," *IEEE C95.*, pp. 1–1991, 1992.

[21] A. Christ, M. Douglas, J. Nadakuduti, and N. Kuster, "Assessing human exposure to electromagnetic fields from wireless power transmission systems," *Proc. IEEE.*, vol. 101, no. 6, pp. 1482–1493, 2013.

[22] E. G. Kilinc, C. Dehollain, and F. Maloberti, "Design and optimization of inductive power transmission for implantable sensor system," *XIth Int. Workshop Symbolic Numer. Methods, Model. Appl. Circuit Design*, pp. 1–5, Oct. 2010.

[23] A. Ibrahim and M. Kiani, "A figure-of-merit for design and optimization of inductive power transmission links for millimeter-sized biomedical implants," *IEEE Trans. Biomed. Circuits Syst.*, vol. 10, no. 6, pp. 1100–1111, Dec. 2016.

[24] U. M. Jow and M. Ghovanloo, "Design and optimization of printed spiral coils for efficient transcutaneous inductive power transmission," *IEEE Trans. Biomed. Circuits Syst.*, vol. 1, no. 3, pp. 193–202, Sep. 2007.

[25] P. Feng, T. G. Constandinou, P. Yeon, and M. Ghovanloo, "Millimeter-scale integrated and wirewound coils for powering implantable neural microsystems," in *Proc. IEEE Biomed. Circuits Syst. Conf.*, Oct. 2017, pp. 1–4.

[26] U. M. Jow and M. Ghovanloo, "Modeling and optimization of printed spiral coils in air, saline, and muscle tissue environments," *IEEE Trans. Biomed. Circuits Syst.*, vol. 3, no. 5, pp. 339–347, Oct. 2009.

[27] M. Schormans, V. Valente, and A. Demosthenous, "Practical inductive link design for biomedical wireless power transfer: A tutorial," *IEEE Trans. Biomed. Circuits Syst.*, vol. 12, no. 5, pp. 1112–1130, Oct. 2018.

[28] S. S. Mohan, M. del Mar Hershenson, S. P. Boyd, and T. H. Lee, "Simple accurate expressions for planar spiral inductances," *IEEE J. Solid-State Circuits*, vol. 34, no. 10, pp. 1419–1424, Oct. 1999.

[29] P. Pieters *et al.*, "Accurate modeling of high-Q spiral inductors in thin-film multilayer technology for wireless telecommunication applications," *IEEE Trans. Microw. Theory Techn.*, vol. 49, no. 4, pp. 589–599, Apr. 2001.

[30] H. A. Wheeler, "Formulas for the skin effect," *Proc. IRE*, vol. 30, no. 9, pp. 412–424, 1942.

[31] W. B. Kuhn and N. M. Ibrahim, "Analysis of current crowding effects in multiturn spiral inductors," *IEEE Trans. Microw. Theory Techn.*, vol. 49, no. 1, pp. 31–38, Jan. 2001.

[32] S. Gevorgian, H. Berg, H. Jacobsson, and T. Lewin, "Basic parameters of coplanar-strip waveguides on multilayer dielectric/semiconductor substrates, Part 1: High permittivity superstrates," *IEEE Microw. Mag.*, vol. 4, no. 2, pp. 60–70, Jun. 2003.

[33] I. J. Bahl and R. Garg, "Simple and accurate formulas for a microstrip with finite strip thickness," *Proc. IEEE.*, vol. 65, no. 11, pp. 1611–1612, Nov. 1977.

[34] L. W. Ritchey and S. Edge, "A survey and tutorial of dielectric materials used in the manufacture of printed circuit boards," *Circuitree Mag.*, 1999.

[35] A. Ibrahim and M. Kiani, "Safe inductive power transmission to millimeter-sized implantable microelectronics devices," in *Proc. Int. Conf. IEEE Eng. Med. Biol. Soc.*, 2015, pp. 817–820.

[36] D. Ahn and M. Ghovanloo, "Optimal design of wireless power transmission links for millimeter-sized biomedical implants," *IEEE Trans. Biomed. Circuits Syst.*, vol. 10, no. 1, pp. 125–137, Feb. 2016.

[37] E. Moradi, T. Björninen, L. Sydänheimo, L. Ukkonen, and J. M. Rabaey, "Antenna design for implanted tags in wireless brain machine interface system," in *Proc. IEEE Antennas Propag. Soc. Int. Symp.*, Jul. 2013, pp. 2083–2084.

[38] S. A. Mirbozorgi, P. Yeon, and M. Ghovanloo, "Robust wireless power transmission to mm-sized free-floating distributed implants," *IEEE Trans. Biomed. Circuits Syst.*, vol. 11, no. 3, pp. 692–702, Jun. 2017.

[39] A. Khalifa *et al.*, "The microbead: A 0.009 mm 3 implantable wireless neural stimulator," *IEEE Trans. Biomed. Circuits Syst.*, vol. 13, no. 5, pp. 971–985, 2019.

[40] J. Lee *et al.*, "An implantable wireless network of distributed microscale sensors for neural applications," in *Proc. 9th Int. IEEE/EMBS Conf. Neural Eng.*, Mar. 2019, pp. 871–874.

[41] N. C. Kuo, B. Zhao, and A. M. Niknejad, "Equation-based optimization for inductive power transfer to a miniature CMOS rectenna," *IEEE Trans. Microw. Theory Techn.*, vol. 66, no. 5, pp. 2393–2408, May 2018.

[42] W. Biederman *et al.*, "A fully-integrated, miniaturized (0.125 mm^2) 10.5 μW wireless neural sensor," *IEEE J. Solid-State Circuits*, vol. 48, no. 4, pp. 960–970, 2013.

[43] S. Liu, J. Su, and J. Lai, "Accurate expressions of mutual inductance and their calculation of archimedean spiral coils," *Energies.*, vol. 12, no. 10, 2019.

[44] Y. Cheng and Y. Shu, "A new analytical calculation of the mutual inductance of the coaxial spiral rectangular coils," *IEEE Trans. Magn.*, vol. 50, no. 4, pp. 1–6, Apr. 2014.

[45] R. R. Harrison, "Designing efficient inductive power links for implantable devices," in *Proc. IEEE Int. Symp. Circuits Syst.*, May 2007, pp. 2080–2083.

[46] U. M. Jow, M. Kiani, X. Huo, and M. Ghovanloo, "Towards a smart experimental arena for long-term electrophysiology experiments," *IEEE Trans. Biomed. Circuits Syst.*, vol. 6, no. 5, pp. 414–423, Oct. 2012.

[47] A. Ibrahim and M. Kiani, "Inductive power transmission to millimeter-sized biomedical implants using printed spiral coils," in *Proc. 38th Annu. Int. Conf. IEEE Eng. Med. Biol. Soc.*, Aug. 2016, pp. 4800–4803.

[48] B. Zhao, N. Kuo, B. Liu, Y. Li, L. Iotti, and A. M. Niknejad, "A batteryless padless crystalless 116 μm × 116 μm "diele," near-field radio with on-chip coil antenna," *IEEE J. Solid-State Circuits*, vol. 55, no. 2, pp. 249–260, 2020.

[49] S. Atluri and M. Ghovanloo, "Design of a wideband power-efficient inductive wireless link for implantable biomedical devices using multiple carriers," *Conf. Proc. 2nd Int. IEEE EMBS Conf. Neural Eng.*, pp. 533–537, Mar. 2005.

[50] W. Ye, L. Chen, F. Liu, X. Chen, and X. Wang, "Analysis and optimization of 3-coil magnetically coupled resonant wireless power transfer system for stable power transmission," *IEEE Energy Convers. Congr. Expo.*, pp. 2584–2589, Oct. 2017.

[51] Y. Jia, Y. Gong, A. Weber, W. Li, and M. Ghovanloo, "A mm-sized free-floating wireless implantable opto-electro stimulation device," *Micromachines*, vol. 11, no. 6, p. 621, 2020.

[52] P. C. Ghosh, P. Sadhu, and A. Ghosh, "Analysis of a three-coil contactless power transfer system for high-power applications," *J. Chin. Inst. Eng.*, vol. 42, no. 3, pp. 1100–1111, 2019.

[53] M. Kiani, U. M. Jow, and M. Ghovanloo, "Design and optimization of a 3-coil inductive link for efficient wireless power transmission," *IEEE Trans. Biomed. Circuits Syst.*, vol. 5, no. 6, pp. 579–591, Dec. 2011.

[54] S. A. Mirbozorgi, P. Yeon, and M. Ghovanloo, "Robust wireless power transmission to mm-sized free-floating distributed implants," *IEEE Trans. Biomed. Circuits Syst.*, vol. 11, no. 3, pp. 692–702, 2017.

[55] J. Lee *et al.*, "Wireless power and data link for ensembles of sub-mm scale implantable sensors near 1 GHz," in *Proc. IEEE Biomed. Circuits Syst. Conf.*, Oct. 2018, pp. 1–4.

[56] P. Yeon, S. A. Mirbozorgi, and M. Ghovanloo, "Optimal design of a 3-coil inductive link for millimeter-sized biomedical implants," in *Proc. IEEE Biomed. Circuits Syst. Conf.*, Oct. 2016, pp. 396–399.

[57] A. S. Poon, S. O'Driscoll, and T. H. Meng, "Optimal frequency for wireless power transmission into dispersive tissue," *IEEE Trans. Antennas Propag.*, vol. 58, no. 5, pp. 1739–1750, May 2010.

[58] F. Laiwalla *et al.*, "A distributed wireless network of implantable sub-mm cortical microstimulators for brain-computer interfaces," in *Proc. 41st Annu. Int. Conf. IEEE Eng. Med. Biol. Soc.*, Jul. 2019, pp. 6876–6879.

[59] J. Lee *et al.*, "Wireless ensembles of sub-mm microimplants communicating as a network near 1 ghz in a neural application," *bioRxiv*, 2020.

[60] P. Feng and T. G. Constandinou, "Robust wireless power transfer to multiple mm-scale freely-positioned neural implants," in *Proc. IEEE Biomed. Circuits Syst. Conf.*, Oct. 2018, pp. 1–4.

[61] P. Feng, M. Maslik, and T. G. Constandinou, "EM-lens enhanced power transfer and multi-node data transmission for implantable medical devices," in *Proc. IEEE Biomed. Circuits Syst. Conf.*, Oct. 2019, pp. 1–4,.

[62] F. Merli, B. Fuchs, J. R. Mosig, and A. K. Skrivervik, "The effect of insulating layers on the performance of implanted antennas," *IEEE Trans. Antennas Propag.*, vol. 59, no. 1, pp. 21–31, Jan. 2011.

[63] A. M. Sodagar and P. Amiri, "Capacitive coupling for power and data telemetry to implantable biomedical microsystems," in *Proc. 4th Int. IEEE/EMBS Conf. Neural Eng., NER*, 2009, pp. 411–414.

[64] S. Nag, A. Koruprolu, S. M. Saikh, R. Erfani, and P. Mohseni, "Auto-resonant tuning for capacitive power and data telemetry using flexible patches," *IEEE Trans. Circuits Syst. II: Exp. Briefs*, vol. 67, no. 10, pp. 1804–1808, Oct. 2020.

[65] M. Takhti, F. Asgarian, and A. M. Sodagar, "Modeling of a capacitive link for data telemetry to biomedical implants," in *Proc. IEEE Biomed. Circuits Syst. Conf.*, Nov. 2011, pp. 181–184.

[66] R. Erfani, F. Marefat, A. M. Sodagar, and P. Mohseni, "Transcutaneous capacitive wireless power transfer (C-WPT) for biomedical implants," *Proc.-IEEE Int. Symp. Circuits Syst.*, 2017.

[67] R. Jegadeesan, K. Agarwal, Y. X. Guo, S. C. Yen, and N. V. Thakor, "Wireless power delivery to flexible subcutaneous implants using capacitive coupling," *IEEE Trans. Microw. Theory Techn.*, vol. 65, no. 1, pp. 280–292, Jan. 2017.

[68] R. Erfani, F. Marefat, and P. Mohseni, "Biosafety considerations of a capacitive link for wireless power transfer to biomedical implants," in *Proc. IEEE Biomed. Circuits Syst. Conf.*, Oct. 2018, pp. 1–4.

[69] R. Narayanamoorthi, "Modeling of capacitive resonant wireless power and data transfer to deep biomedical implants," *IEEE Trans. Compon., Packag. Manuf. Technol.*, vol. 9, no. 7, pp. 1253–1263, Jul. 2019.

[70] R. Erfani, F. Marefat, A. M. Sodagar, and P. Mohseni, "Modeling and experimental validation of a capacitive link for wireless power transfer to biomedical implants," *IEEE Trans. Circuits Syst. II: Exp. Briefs*, vol. 65, no. 7, pp. 923–927, Jul. 2018.

[71] R. Erfani, F. Marefat, A. M. Sodagar, and P. Mohseni, "Modeling and characterization of capacitive elements with tissue as dielectric material for wireless powering of neural implants," *IEEE Trans. Neural Syst. Rehabil. Eng.*, vol. 26, no. 5, pp. 1093–1099, May 2018.

[72] F. Marefat, R. Erfani, K. L. Kilgore, and P. Mohseni, "A 280 μw 108db dr readout ic with wireless capacitive powering using a dual-output regulating rectifier for implantable ppg recording," in *Proc. IEEE Int. Solid-State Circuits Conf.*, 2020, pp. 412–414.

[73] R. Sedehi *et al.*, "A wireless power method for deeply implanted biomedical devices via capacitively-coupled conductive power transfer," *IEEE Trans. Power Electron.*, vol. 36, no. 2, pp. 1870–1882, Feb. 2021.

[74] F. Lu, H. Zhang, and C. Mi, "A review on the recent development of capacitive wireless power transfer technology," *Energies*, vol. 10, no. 11, 2017.

[75] L. J. Zou, A. P. Hu, and Y. G. Su, "A single-wire capacitive power transfer system with large coupling alignment tolerance," in *Proc. IEEE PELS Workshop Emerging Technol.: Wireless Power Transfer*, May 2017, pp. 93–98.

[76] L. J. Zou, Q. Zhu, C. W. Van Neste, and A. P. Hu, "Modelling single-wire capacitive power transfer system with strong coupling to ground," *IEEE J. Emerg. Sel. Topics Power Electron.*, 2019.

[77] H. Basaeri, Y. Yu, D. Young, and S. Roundy, "Acoustic power transfer for biomedical implants using piezoelectric receivers: effects of misalignment and misorientation," *J. Micromech. Microeng.*, vol. 29, no. 8, 2019.

[78] S. Ozeri and D. Shmilovitz, "Ultrasonic transcutaneous energy transfer for powering implanted devices," *Ultrasonics*, vol. 50, no. 6, pp. 556–566, May 2010.

[79] D. Callens, C. Bruneel, and J. Assaad, "Matching ultrasonic transducer using two matching layers where one of them is glue," *Ndt & E Int.*, vol. 37, no. 8, pp. 591–596, 2004.

[80] S. Roundy, P. K. Wright, and J. M. Rabaey, "Energy scavenging for wireless sensor networks," pp. 45–47, 2003.

[81] H. S. Tzou, *Piezoelectric shells*. Berlin, Germany: Springer, 1993.

[82] N. Guo, "The vibration characteristics of piezoelectric discs," Ph.D. dissertation, 1989.

[83] M. Meng and M. Kiani, "Design and optimization of ultrasonic wireless power transmission links for millimeter-sized biomedical implants," *IEEE Trans. Biomed. Circuits Syst.*, vol. 11, no. 1, pp. 98–107, Feb. 2017.

[84] M. Meng, A. Ibrahim, and M. Kiani, "Design considerations for ultrasonic power transmission to millimeter-sized implantable microelectronics devices," in *Proc. IEEE Biomed. Circuits Syst. Conf.*, Oct. 2015, pp. 1–4.

[85] D. Ensminger and L. J. Bond, "Ultrasonics: Fundamentals, technologies, and applications," 2011.

[86] R. Krimholtz, D. A. Leedom, and G. L. Matthaei, "New equivalent circuits for elementary piezoelectric transducers," *Electron. Lett.*, vol. 6, no. 13, pp. 398–399, 1970.

[87] W. P. Mason, "Electromechanical transducers and wave filters," 1948.

[88] H. Basaeri, D. B. Christensen, and S. Roundy, "A review of acoustic power transfer for bio-medical implants," *Smart Mater. Struct.*, vol. 25, no. 12, 2016.

[89] A. Denisov and E. Yeatman, "Ultrasonic vs. inductive power delivery for miniature biomedical implants," in *Proc. Int. Conf. Body Sensor Netw.*, Jun. 2010, pp. 84–89.

[90] J. Charthad, M. J. Weber, T. C. Chang, and A. Arbabian, "A mm-sized implantable medical device (IMD) with ultrasonic power transfer and a hybrid bi-directional data link," *IEEE J. Solid-State Circuits*, vol. 50, no. 8, pp. 1741–1753, 2015.

[91] S. H. Song, A. Kim, and B. Ziaie, "Omnidirectional ultrasonic powering for millimeter-scale implantable devices," *IEEE Trans. Biomed. Eng.*, vol. 62, no. 11, pp. 2717–2723, Nov. 2015.

[92] D. Seo, J. M. Carmena, J. M. Rabaey, M. M. Maharbiz, and E. Alon, "Model validation of untethered, ultrasonic neural dust motes for cortical recording," *J. Neurosci. Methods.*, vol. 244, pp. 114–122, 2015.

[93] T. C. Chang, M. J. Weber, J. Charthad, S. Baltsavias, and A. Arbabian, "End-to-end design of efficient ultrasonic power links for scaling towards submillimeter implantable receivers," *IEEE Trans. Biomed. Circuits Syst.*, vol. 12, no. 5, pp. 1100–1111, 10 2018.

[94] M. Meng and M. Kiani, "A hybrid inductive-ultrasonic link for wireless power transmission to millimeter-sized biomedical implants," *IEEE Trans. Circuits Syst. II: Exp. Briefs*, vol. 64, no. 10, pp. 1137–1141, Oct. 2017.

[95] D. K. Piech *et al.*, "A wireless millimetre-scale implantable neural stimulator with ultrasonically powered bidirectional communication," *Nature Biomed. Eng.*, vol. 4, no. 2, pp. 207–222, 2020.

[96] D. Seo *et al.*, "Ultrasonic beamforming system for interrogating multiple implantable sensors," in *Proc.37th Annu. Int. Conf. IEEE Eng. Med. Biol. Soc.*, Aug. 2015, pp. 2673–2676.

[97] A. Bertrand *et al.*, "Beamforming approaches for untethered, ultrasonic neural dust motes for cortical recording: a simulation study," in *Proc. 36th Annu. Int. Conf. IEEE Eng. Med. Biol. Soc.*, Aug. 2014, pp. 2625–2628.

[98] D. B. Christensen, H. Basaeri, and S. Roundy, "A computationally efficient technique to model depth, orientation and alignment via ray tracing in acoustic power transfer systems," *Smart Mater. Struct.*, vol. 26, no. 12, 2017.

[99] M. Meng and M. Kiani, "Self-image-guided ultrasonic wireless power transmission to millimeter-sized biomedical implants," in *Proc. 41st Annu. Int. Conf. IEEE Eng. Med. Biol. Soc.*, 2019, pp. 364–367.

[100] A. Ibrahim, M. Meng, and M. Kiani, "A comprehensive comparative study on inductive and ultrasonic wireless power transmission to biomedical implants," *IEEE Sens. J.*, vol. 18, no. 9, pp. 3813–3826, May 2018.

[101] D. Seo, "Neural dust: Ultrasonic biological interface," *eScholarship*, University of California, 2016.

[102] J. Li and C. T. Chan, "Double-negative acoustic metamaterial," *Phys. Rev. E*, vol. 70, no. 5, 2004.

[103] R. Erfani, F. Marefat, S. Nag, and P. Mohseni, "A 1-10-mhz frequency-aware cmos active rectifier with dual-loop adaptive delay compensation and >230-mw output power for capacitively powered biomedical implants," *IEEE J. Solid-State Circuits*, vol. 55, no. 3, pp. 756–766, 2020.

Gian Luca Barbruni was born in Sanremo (IM), Italy in 1995. He received the B.Sc. and M.Sc. degrees in biomedical engineering from Politecnico di Torino, Turin, Italy, in 2017 and 2019, respectively. He is currently working toward the Ph.D. degree in microsystems and microelectronics, Campus Biotech, Geneva, Ecole Polytechnique Fédérale de Lausanne, Lausanne, Switzerland. He was a Research Associate with the Department of Electronic Engineering, MiNES (Micro&Nano Electronic Systems) Laboratory, Politecnico di Torino. His Ph.D. project is focused on the development of miniaturised neuroprosthesis device for artificial vision. His current research interests include biosensors, neural prosthesis, analog and digital CMOS design, wireless power transfer and data communication, ultra-low-power, and miniaturised CMOS integrated circuits for the development of innovative biomedical systems.

Paolo Motto Ros (Member, IEEE) received the Engineering and Ph.D. degrees in electronic engineering from the Politecnico di Torino, Torino, Italy, in 2005 and 2009, respectively. He is Senior Postdoctoral Researcher with Politecnico di Torino (Torino, Italy), Dipartimento di Elettronica e Telecomunicazioni, with the MiNES (Micro&Nano Electronic Systems) group. From 2009 to 2012, he was with Neuronica Laboratory (Dipartimento di Elettronica, Politecnico di Torino) as Postdoc Researcher, working on assistive technologies, computer vision and learning machines projects (jointly with, 2006–2011, Istituto Nazionale Fisica Nucleare, INFN, Italy). From 2012 to 2019, he was with Istituto Italiano di Tecnologia (Center for Space Human Robotics, CSHR, Torino, Italy, and, since 2016, Electronic Design Laboratory, EDL, Genova, Italy) as Senior (since 2014) Postdoc Researcher, working on bioinspired electronics for biomedical and humanoid robotic applications. He joined the Politecnico di Torino, Dipartimento di Elettronica e Telecomunicazioni, in 2019. He current research interests include event-driven digital integrated circuits, architectures, and systems; low-power smart sensor networks; bio-inspired electronics; and biomedical and humanoid robotic applications. Dr. Ros is member of the Circuits And Systems Society. He was member of the organizing staff of the IEEE BioCAS 2017 conference, and member of the organizing committee of the IEEE ICECS 2019 conference.

Danilo Demarchi (Senior Member, IEEE) received the Engineering and Ph.D. degrees in electronics engineering from Politecnico di Torino, Torino, Italy, in 1991 and 1995, respectively. He is currently an Associate Professor with Politecnico di Torino, Department of Electronics and Telecommunications. Visiting Professor with EPFL Lausanne and with Tel Aviv University. In 2018, he was visiting Scientist at MIT and Harvard Medical School. He has authored and coauthored five patents and more than 250 scientific publications in international journals and peer-reviewed conference proceedings. He is leading the MiNES (Micro&Nano Electronic Systems, http://mines.polito.it) Laboratory of Politecnico di Torino. Dr. Demarchi was member of the BioCAS Technical Committee, Associate Editor of the *Transactions on Biomedical Circuits and Systems*, Associate Editor for the IEEE SENSORS and of the *Springer Journal BioNanoScience*, General Chair of Biomedical Circuits and Systems Conference edition in Torino, October 2017, and Founder of IEEE FoodCAS Workshop (Circuits and Systems for the Food Chain).

Sandro Carrara (Fellow, IEEE) received diploma degree in electronics from National Institute of Technology, Albenga, Italy, the master's degree in physics from University of Genoa, Genoa, Italy, and the Ph.D. degree in biochemistry and biophysics from University of Padua, Padua, Italy. He has authored and coauthored seven books with prestigious publishers such as Springer/NATURE and Cambridge University Press. He has more than 300 scientific publications and is author of 14 patents. He is Editor-in-Chief of the IEEE Sensors Journal, the largest journal among 180 IEEE publications, and Associate Editor for the IEEE TRANSACTIONS ON BIOMEDICAL CIRCUITS AND SYSTEMS. He is a member of the IEEE Sensors Council and his Executive Committee. He was a member of the Board of Governors of the IEEE Circuits And Systems Society. He is the recipient of the IEEE Sensors Council Technical Achievement Award. He is faculty at the EPFL in Lausanne (CH), Former Professor with the Universities of Genoa and Bologna.

Diego Ghezzi (Member, IEEE) received the M.Sc. degree in biomedical engineering and the Ph.D. degree in bioengineering from Politecnico di Milano, Milan, Italy, in 2004 and 2008, respectively. From 2008 to 2013, he completed his Postdoctoral Training with Istituto Italiano di Tecnologia in Genova, Department of Neuroscience and Brain Technologies; where he was promoted to Researcher in 2013. In 2015, he was appointed as Tenure-Track Assistant Professor of Bioengineering with the Center for Neuroprosthetics and Institute of Bioengineering of the Ecole Polytechnique Fédérale de Lausanne. He holds the Medtronic Chair in Neuroengineering.